



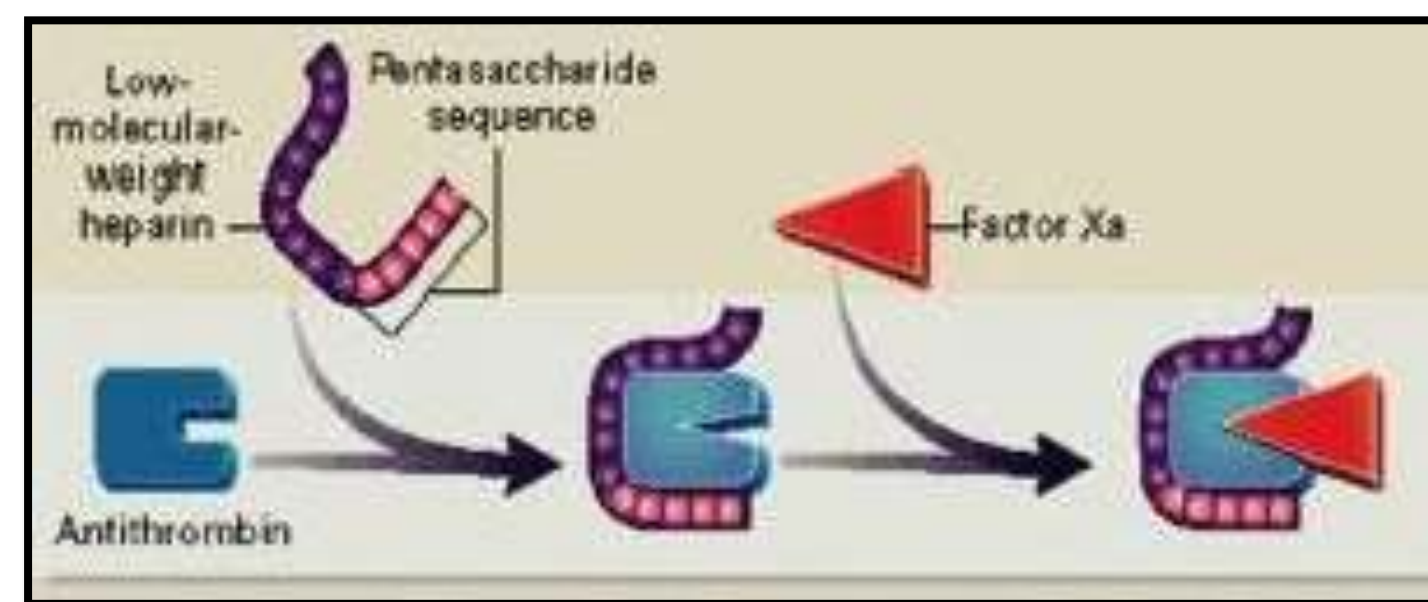
Clinical Effect of Enoxaparin on INR following Hepatobiliary & Gastroesophageal Resection

Matthew W. Kelecy, Jack Rostas MD., Travis Shutt MD. and Robert C.G. Martin MD. PhD.

University of Louisville, Department of Surgery, Division of Surgical Oncology

Background

- Enoxaparin inactivates factor Xa via a complex formed after binding to circulating anti-thrombin III.
- This mechanism is reported to not alter hemostatic measures such as clotting time, PT or PTT.
- To date, no clinical trials have shown a causal relationship between the clinical or pharmacological effects of enoxaparin on INR.
- The aim of our study is to show the clinical effect of enoxaparin on International Normalized Ratio (INR).



Methods

- Three hundred fifty cases were reviewed from IRB approved databases of patients undergoing gastroesophageal or hepatobiliary surgeries for malignancy.
- Forty-two of the patients received 30mg of enoxaparin daily and 247 received 40mg daily for prophylaxis against venous thromboembolism (VTE) starting post-operative day 1.
- 61 patients who did not receive enoxaparin were used as controls. INR levels were recorded for 6 days: pre-operative to 5 days after surgery.

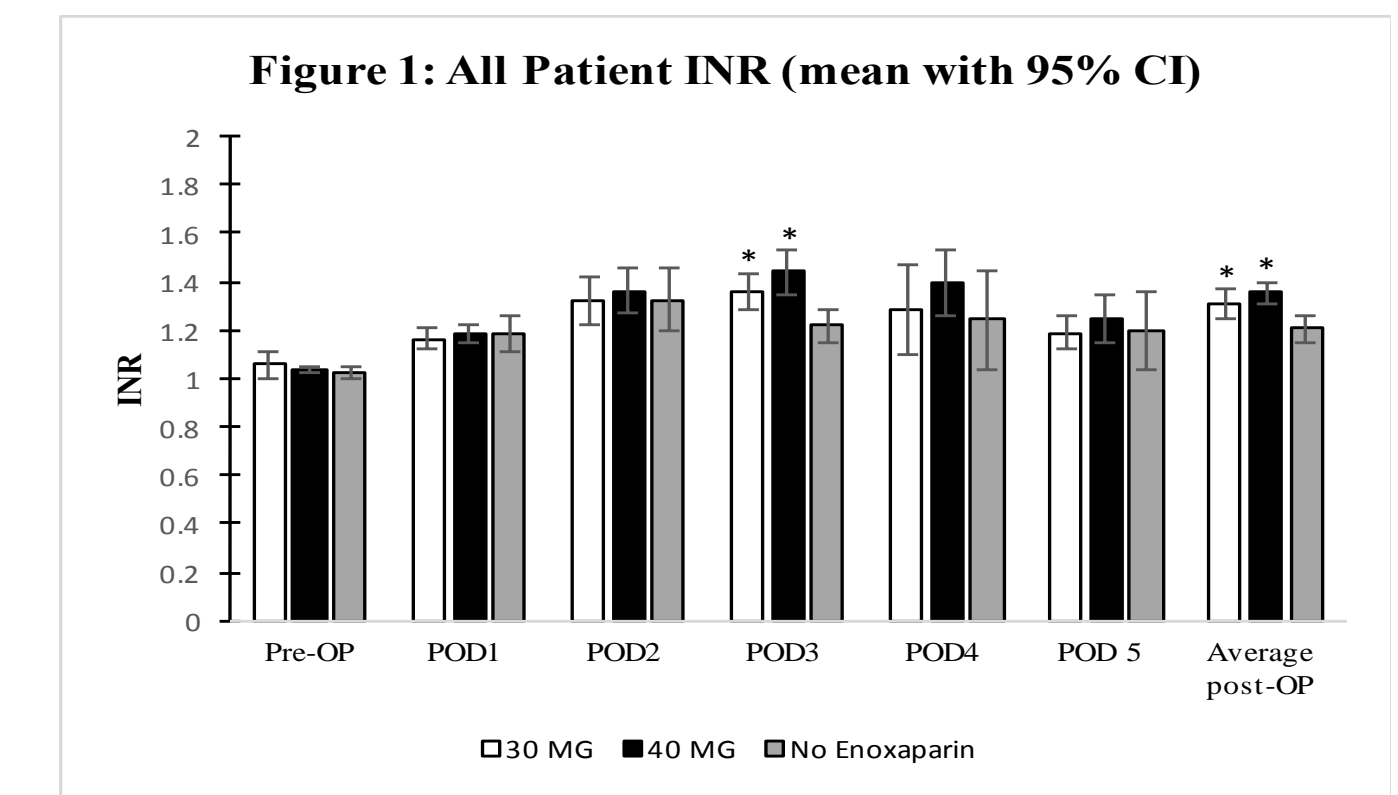
Table 1: Laboratory Measurements (mean ± 95% CI)

	Pre-OP	POD1	POD2	POD3	POD4	POD5	Avg. Post-OP
40 mg enoxaparin							
Hemoglobin (mg/dl)	11.86 ± 0.24†	10.93 ± 0.21	10.30 ± 0.22	9.85 ± 0.20	9.76 ± 0.23	9.60 ± 0.21	10.26 ± 0.190
Platelets (1000/ul)	218.41 ± 13.63	196.51 ± 11.25	178.31 ± 10.10	182.71 ± 11.03	197.12 ± 13.06	206.67 ± 13.45	192.05 ± 11.10
Bilirubin (mg/dl)	0.82 ± 0.10	0.99 ± 0.13	1.10 ± 0.17	1.19 ± 0.21†	1.29 ± 0.28†	1.32 ± 0.27	1.11 ± 0.17†
Creatinine (mg/dl)	0.85 ± 0.04	0.86 ± 0.04	0.86 ± 0.06	0.77 ± 0.04	0.74 ± 0.05	0.73 ± 0.05	0.79 ± 0.04
30 mg enoxaparin							
Hemoglobin (mg/dl)	12.24 ± 0.65	10.65 ± 0.55	10.20 ± 0.55	9.61 ± 0.58	9.73 ± 0.60	9.65 ± 0.48	10.06 ± 0.50
Platelets (1000/ul)	246.11 ± 43.66	215.41 ± 34.68	193.73 ± 35.60	204.35 ± 34.90	222.00 ± 38.97	234.03 ± 43.54	211.25 ± 33.52
Bilirubin (mg/dl)	0.68 ± 0.12	0.75 ± 0.13†	0.75 ± 0.20†	0.78 ± 0.21†	0.85 ± 0.17†	0.92 ± 0.31	0.80 ± 0.15†
Creatinine (mg/dl)	0.87 ± 0.26	0.82 ± 0.17	0.78 ± 0.14	0.73 ± 0.15	0.71 ± 0.16	0.62 ± 0.06†	0.74 ± 0.14
Control							
Hemoglobin (mg/dl)	12.48 ± 0.45	10.84 ± 0.47	10.33 ± 0.47	10.23 ± 0.44	10.20 ± 0.39	10.05 ± 0.36	10.50 ± 0.36
Platelets (1000/ul)	219.43 ± 24.06	184.55 ± 19.77	173.65 ± 19.66	178.81 ± 23.60	194.34 ± 25.08	215.54 ± 31.93	186.17 ± 21.26
Bilirubin (mg/dl)	0.76 ± 0.18	1.29 ± 0.34	1.47 ± 0.50	1.81 ± 0.64	2.04 ± 0.81	1.82 ± 0.86	1.57 ± 0.49
Creatinine (mg/dl)	0.83 ± 0.07	0.89 ± 0.10	0.88 ± 0.16	0.89 ± 0.21	0.80 ± 0.15	0.77 ± 0.13	0.85 ± 0.13

Results

- Median preoperative INR was 1.0 in the 30mg, 40mg, and control groups.
- The average post-operative INR in both the 30 mg and 40 mg groups were both significantly higher than the average post-operative INR of the control group (P=0.015 and P=0.00075 respectively).
- By postoperative day 5 the median INR fell to 1.20 in drug groups.
- Preoperative hemoglobin levels were significantly lower in the 30mg vs control (11.7 vs 12.8; P = 0.026).
- Average post-operative bilirubin was significantly different in the drug groups vs controls; 30 mg vs control: P= 0.008 40 mg vs control P = 0.028. Platelet counts were not different between groups.

Results



Conclusions

- This is the first clinical evidence of the effect of enoxaparin on INR in patients undergoing abdominal surgeries.
- We demonstrate an increase in the INR for patients who received enoxaparin for post-operative VTE prophylaxis.
- Future studies, will evaluate if these increase in INR that occur are clinically relevant or related to lab abnormalities.

Acknowledgements

I would like to thank the NIH R25 Education Grant (R25- CA134283) for Funding this research, my mentor Dr. Robert C.G. Martin for his guidance, and Travis Shutt and Jack Rostas for their assistance in collecting the Data.



LASER-IRRADIATED "BINARY BOMB" NANOPARTICLES ENCAPSULATING GOLD NANORODS AND CHEMOTHERAPEUTICS TO MEDIATE HEPATOCELLULAR CARCINOMA APOPTOSIS



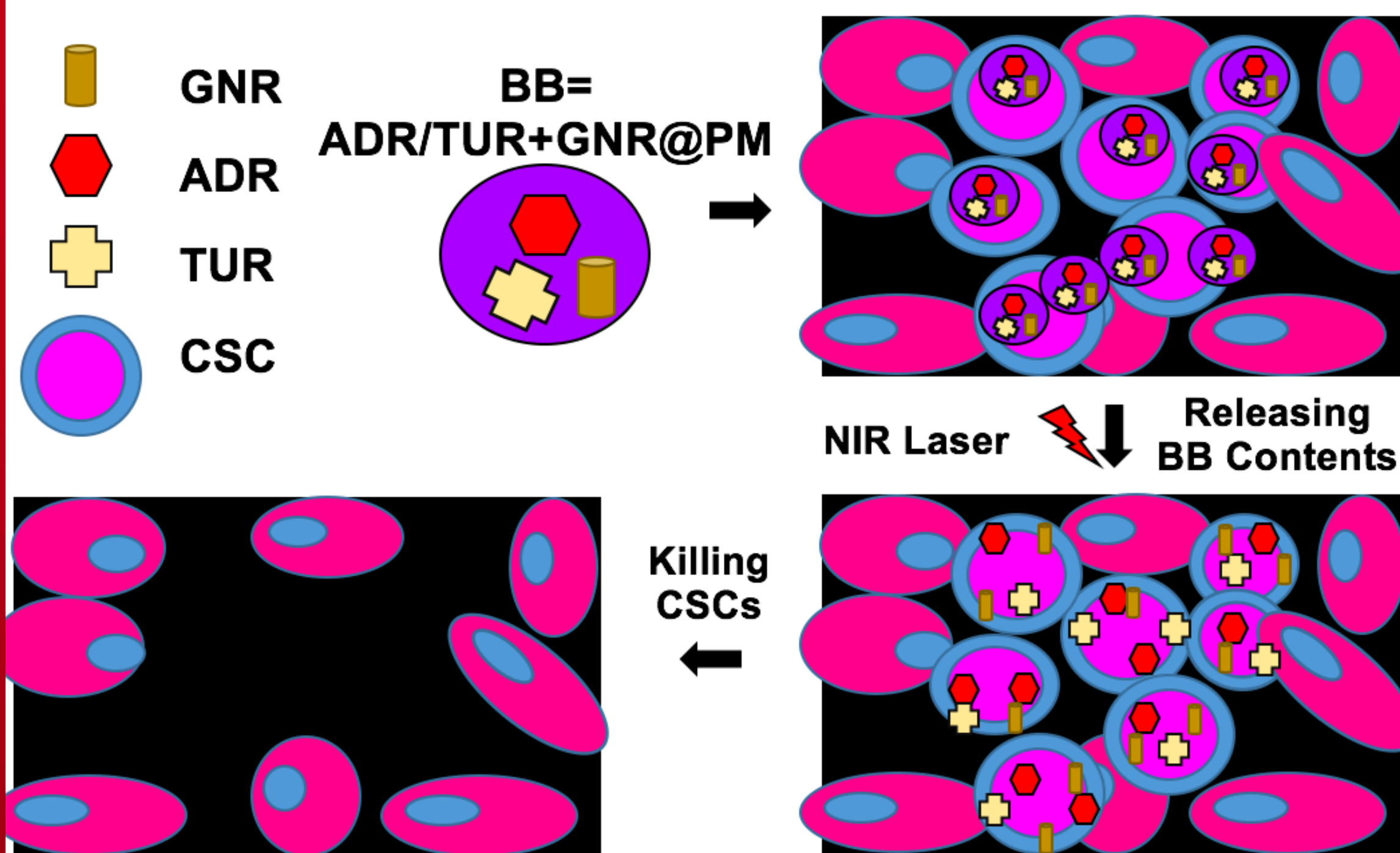
Emily Martin, MEng, Harshul Pandit, MS, Suping Li, MS, Robert CG Martin II, MD, PhD, Yan Li, MD, PhD
Department of Surgery, Division of Surgical Oncology, University of Louisville, Louisville, KY

INTRODUCTION

- Hepatocellular Carcinoma (HCC) is the second leading cause of cancer-related deaths worldwide.
- Evidence indicates Cancer Stem Cells (CSCs) played a key role for HCC therapeutic failure and recurrence.
- Previous work in our group used gold nanorods (GNRs) loaded curcumin to target and kill cancer cells in vitro and in vivo.
- This study aims to target CSCs with GNR based Binary Bombs (BBs), which also contain Adriamycin (ADR) and ar-Turmerone (TUR).

OBJECTIVE AND HYPOTHESIS

- Assess efficacy of BBs in vitro and in vivo and determine downstream cellular events they illicit when inducing HCC cell death.



METHODS

- In vitro HCC cell lines: HepG2 and Hep3B
- Spheroid assay: HCC cells → HCC CSCs
- XTT Cell Viability Assay: to determine metabolically active cells after treatment to find appropriate treatment time for efficacy
- TUNEL (Terminal deoxynucleotidyl transferase dUTP Nick End Labeling): stains for DNA fragmentation
- Western Blot of Caspase-3, 8, & 9; β -catenin; GSK-3 β ; Cyclin D1
- In vivo: HCC tumor-induced murine model
 - Ultrasound → show tumor progression
 - H&E, Silver, and CD133/EpCAM stains

RESULTS

Figure 1. XTT Assay to determine treatment time and efficacy of particles on normal HCC cell lines.

BB treatment group had significantly less cell viability than Untreated (UT) group (#, $p < 0.05$ vs UT) after 24hrs in HepG2 and Hep3B cells.

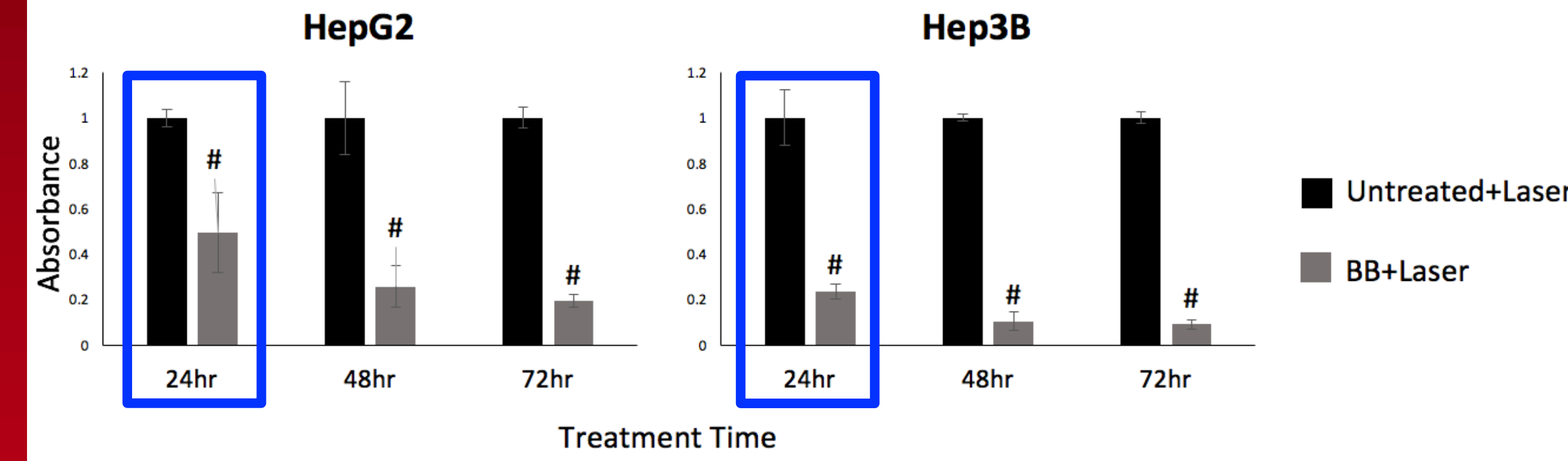


Figure 2. Phenotypic Changes after Spheroid Assay and XTT of Spheroids after Treatment with ADR, TUR, and BB+Laser.

HepG2: Treated groups had significantly less cell viability than untreated group. BB+Laser statistically had the lowest cell viability (#, $p = 0.022$ vs UT)

Hep3B: ADR and BB+Laser had significantly less cell viability than Untreated and TUR groups (#, $p = 0.003$)

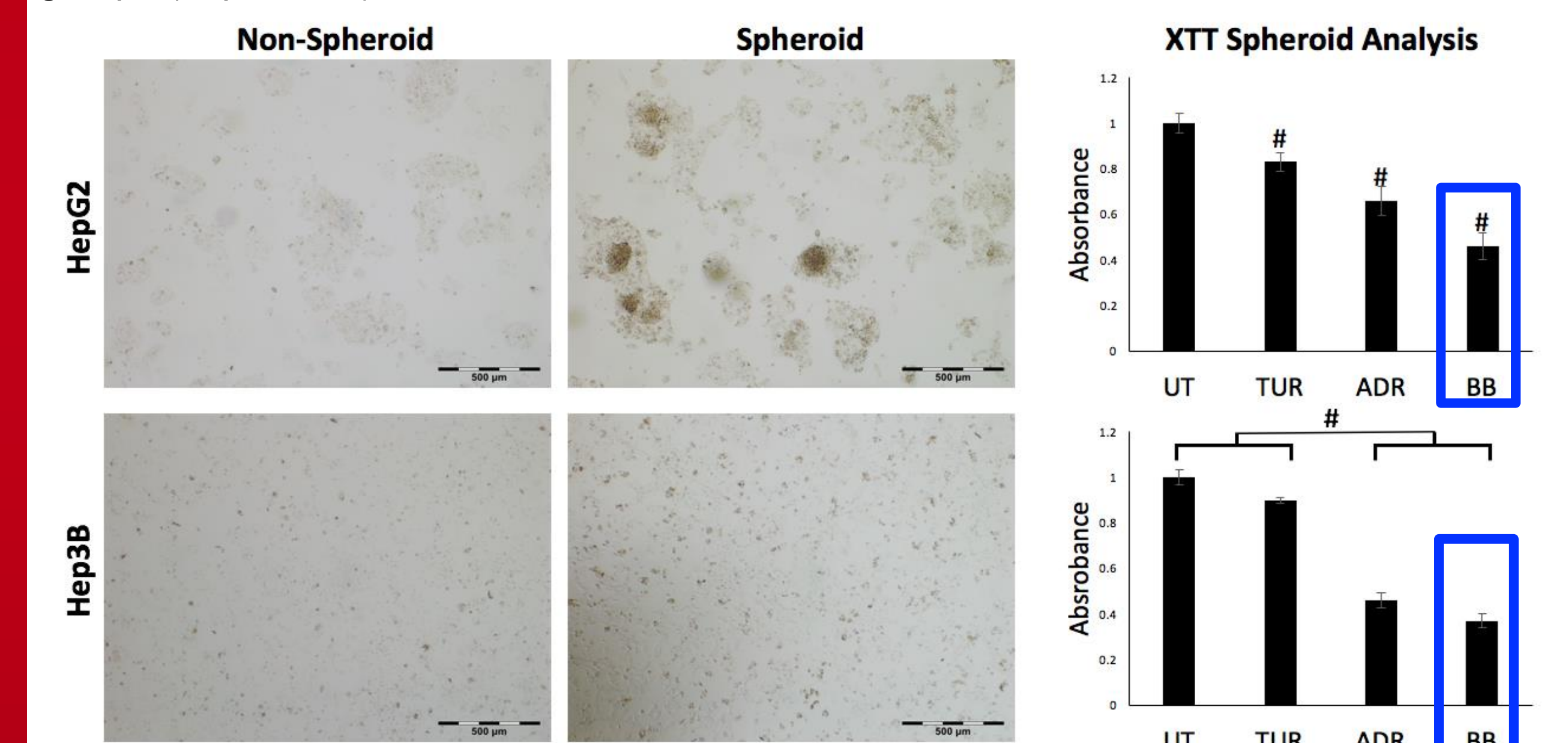
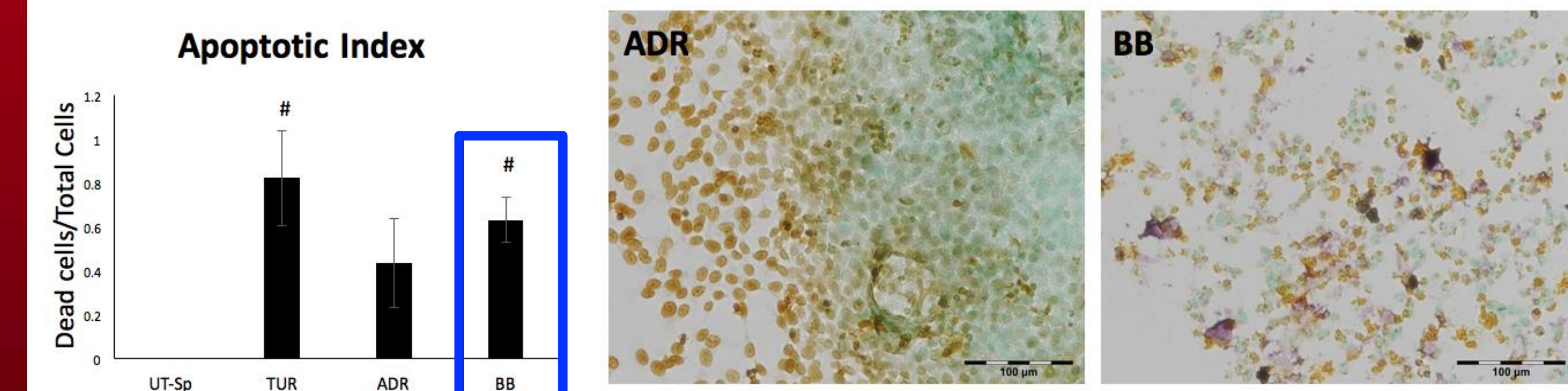


Figure 3. TUNEL stain: HepG2 treated cells.

Untreated and ADR had statistically less DNA fragmentation than TUR and BB+Laser groups (#, $p = 0.039$ vs UT-SP)



CONCLUSIONS

- BB+Laser treatment is more effective in killing HCC-CSCs in 24hrs than TUR and ADR alone in HepG2 cells.
- BB+Laser treatments induce DNA fragmentation, a hallmark of apoptosis, as shown with the TUNEL assay.
- Western analysis indicates the extrinsic pathway is the main apoptotic signaling that BB+Laser treatments invoke when killing HCC-CSCs.
- HCC orthotopic mouse model shows the efficacy of BB+Laser treatments in vivo, as well as their ability to specifically target HCC-CSCs.

Figure 4. Cellular pathways tested to determine molecular targets of BB treatment.

Extrinsic and intrinsic pathways of Apoptosis (Left) and Wnt pathway. * denotes Western analysis, ** denotes TUNEL analysis.

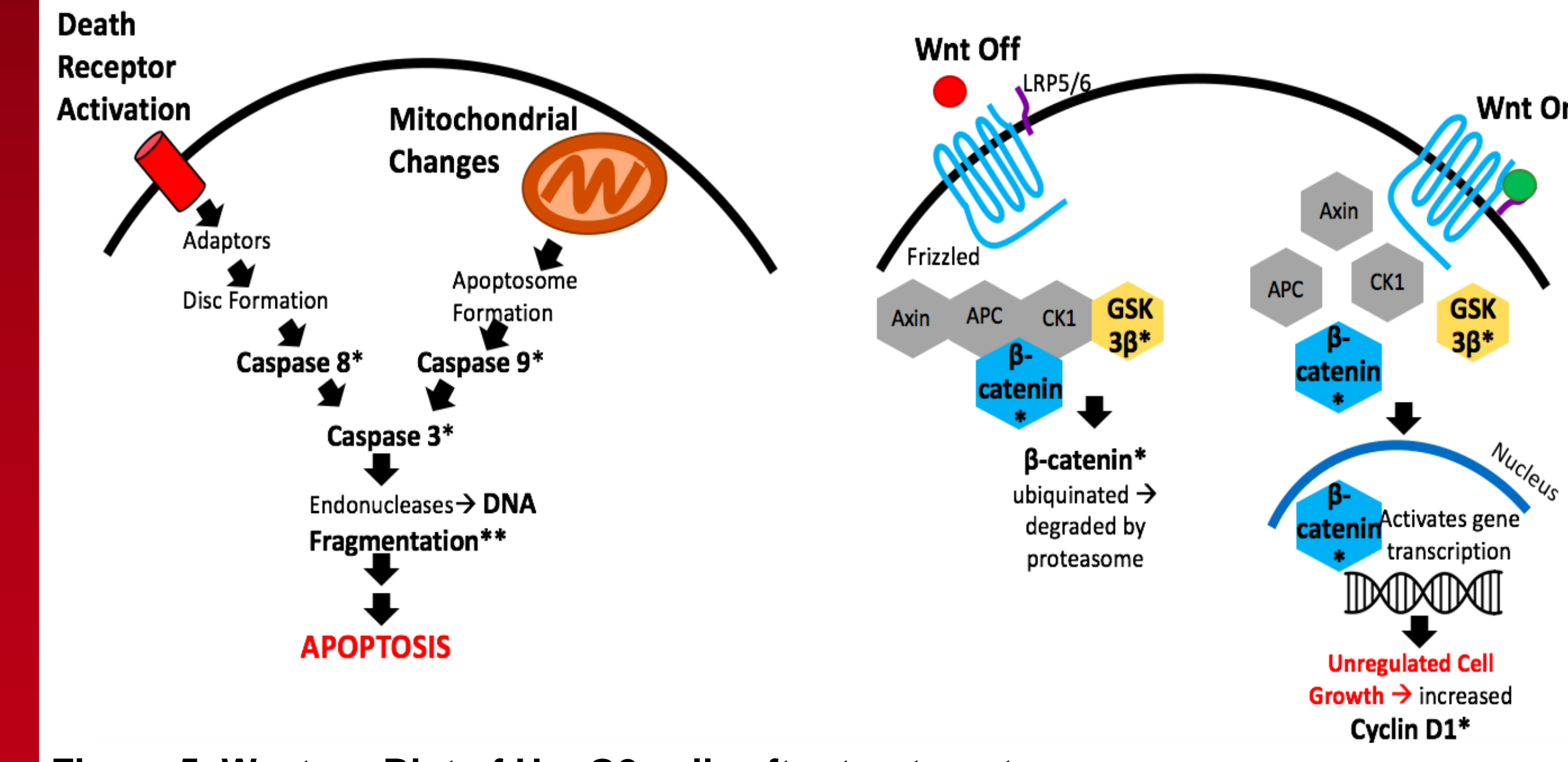


Figure 5. Western Blot of HepG2 cells after treatment.

BB+Laser group had increased β catenin, GSK3 β , Caspase 3, Cyclin D, and Caspase 8 compared to other treatment groups.

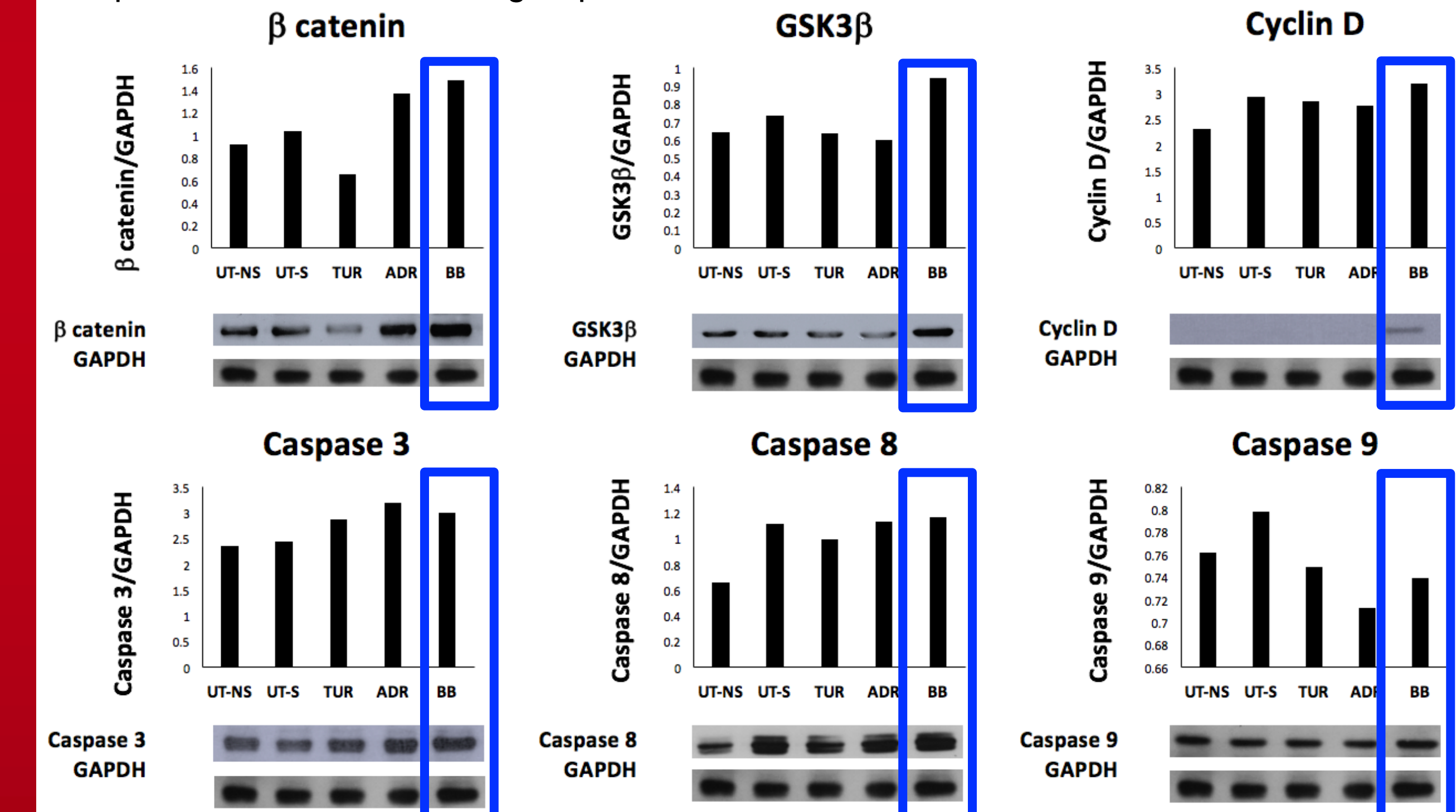
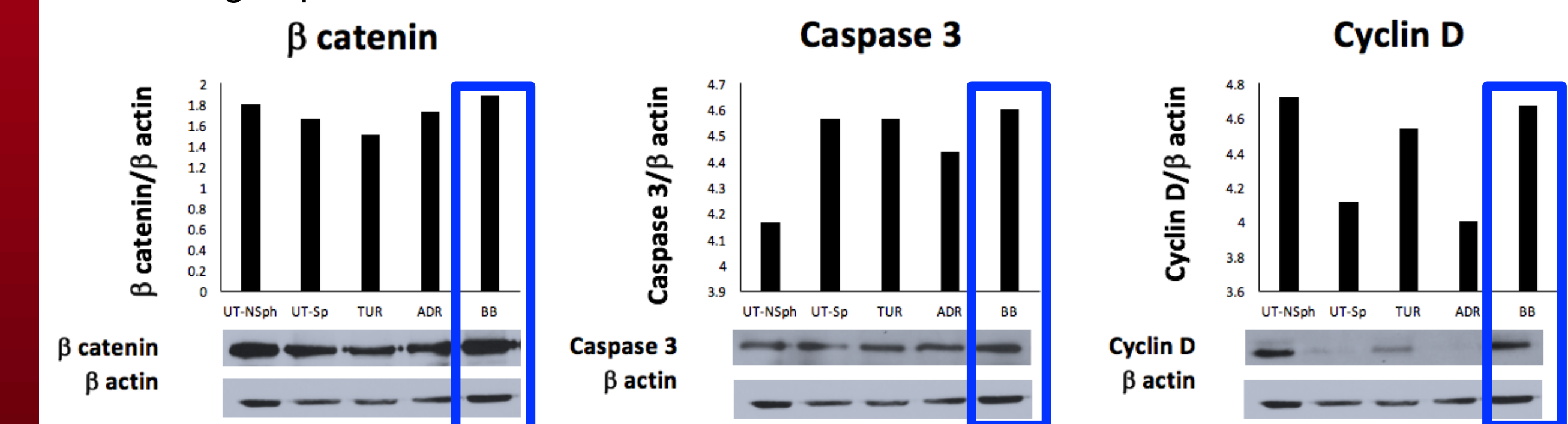


Figure 6. Western Blot of Hep3B cells after treatment.

BB+Laser group had increased β catenin, Caspase 3, and Cyclin D compared to other treatment groups.



RESULTS

Figure 7. Ultrasound of tumor growth in HCC orthotopic mouse tumor model (Right.) Hematoxylin and Eosin stain of murine livers post tumor induction and BB treatment (Below).

Normal shows benign hepatic morphology, Tumor tissue shows tumor growth, BB without laser shows bleeding, BB+Laser shows destruction of tumor, BBL-3d shows tumor necrosis and inflammatory cell infiltration three days post BB+Laser.

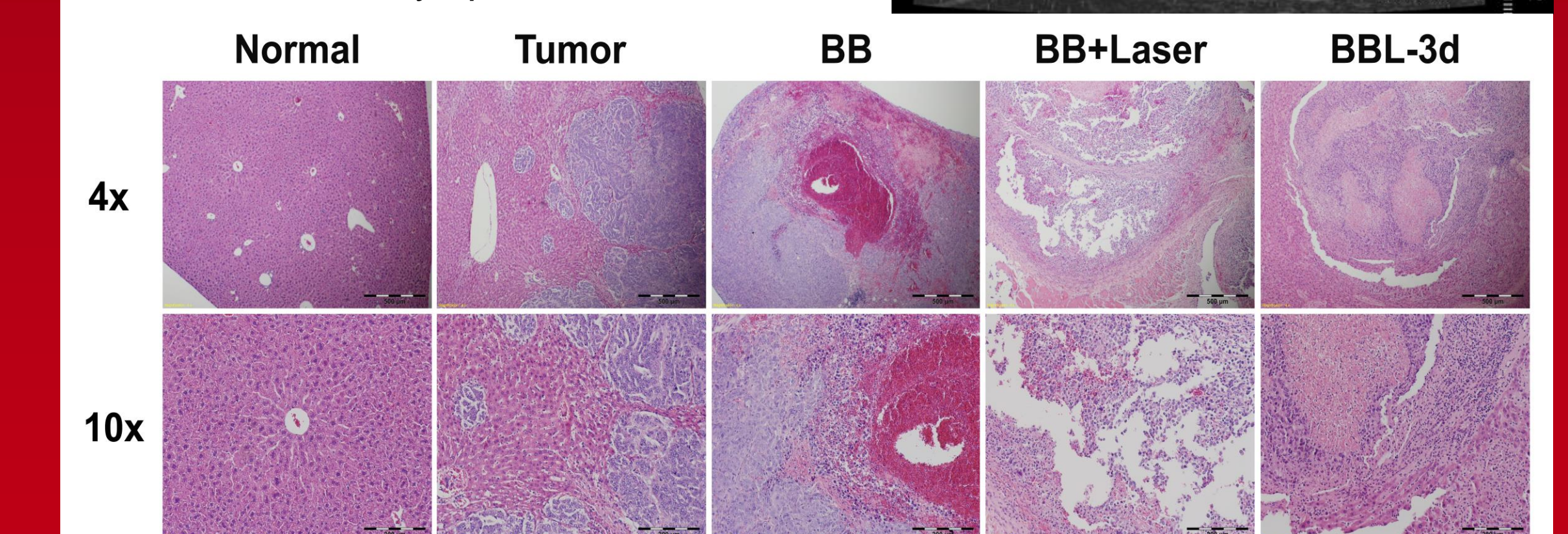
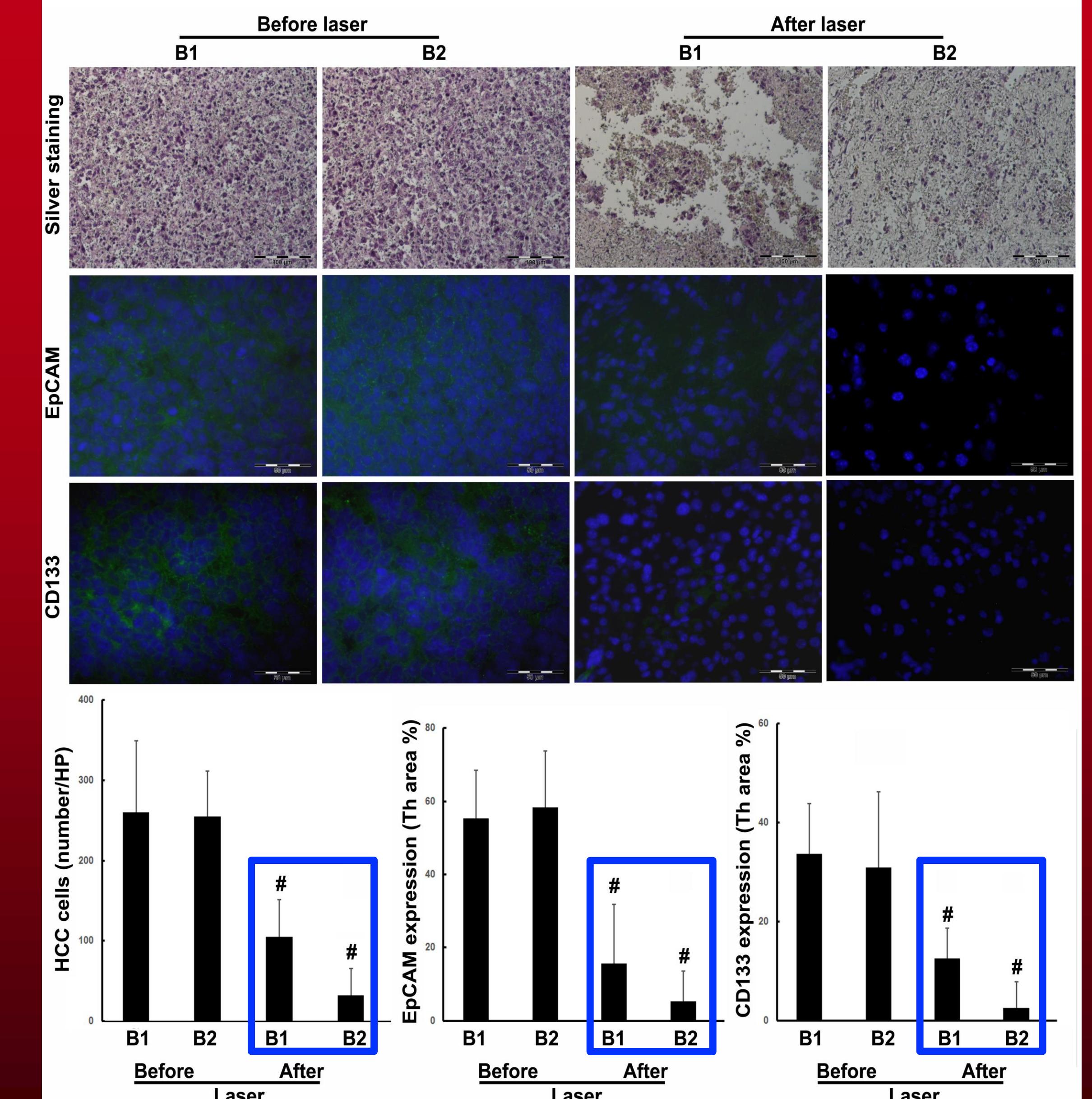


Figure 8. Silver stain, EpCAM stain, and CD133 stains of HCC orthotopic mouse tumor model, as well as HCC cell count after BB treatment, before and after laser (Below).

Silver stain shows BB targeting to HCC cells after BB+Laser treatment. EpCAM and CD133 staining marks presence of CSC in HCC region prior to laser, and shows lack of CSC in HCC region post laser. This is graphically presented below. (#, $p < 0.05$ vs Before laser)



ACKNOWLEDGEMENTS

- Research was supported by the NCI R25-CA134283 grant

LINE-1 ORF-1 protein concentration in healthy women population and endometrial cancer patients

E. Martinez⁴, S.D Jortani PhD², W. Goldsberry MD¹, K. Hosseinejad MD², E. Stauble MD¹

University of Louisville Department of OBGYN¹ University of Louisville Department of Pathology², James Graham Brown Cancer Center³, University of Louisville School of Medicine⁴

Abstract

Introduction

Endometrial cancer is the most common gynecological cancer diagnosed in the U.S. It is of great importance for clinicians to find a reliable biomarker that can be measured in blood in order to diagnose these patients earlier and have a better prognosis. Interspersed nuclear element 1 (LINE-1) is the most abundant retrotransposon in the human body. LINE-1 hyper-activation has been demonstrated in many types of cancer including, colon, prostate, lung, breast and endometrial. LINE-1 activation results in production of Open Reading frame 1 and 2 (ORF-1 and ORF-2).

Objective and hypothesis

In this study serum was obtained from normal and endometrial cancer patients and the amount of ORF1p was quantified. The hypothesis was that ORF1p is going to be higher in cancer patients compare to normal patients.

Methods

Healthy and cancer patients were enrolled from the University of Louisville OBGYN Physician Outpatient Center and James Graham Brown Cancer Center (controls= 24 cases= 2). Blood was collected and serum was separated by spinning down. ORF-1p was measured using a quantitative in-house ELISA with a polyclonal antibody in the department of pathology at University of Louisville.

Results

The mean ORF-1 protein concentration in the normal population was 9.31 (SD=8.25) ng/ml. The cancer patients ORF-1 protein concentration was 0 ng/ml.

Conclusions

The results do not suggest that ORF-1 protein is increased in endometrial cancer patients. However, these data can be used as a baseline of normal patient population for future studies. Disadvantages of this study include a small sample population because of a lack of time to recruit healthy women and endometrial cancer patients.

Introduction

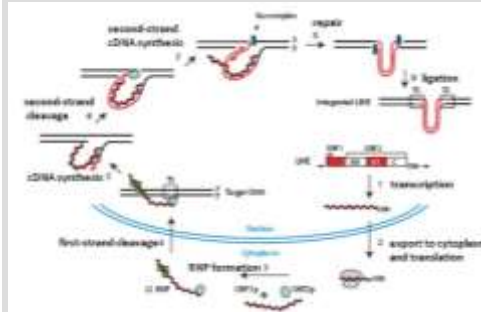
Endometrial cancer is the most common gynecological cancer in the U.S. There are 54,870 cases diagnosed in the United States and 10,170 pts die annually. Although it mainly affects postmenopausal women there are other risk factors such as obesity, altered menstrual cycles, infertility, tamoxifen use, among others.

Abnormal uterine bleeding is present in approximately 75 to 90 percent of women with endometrial carcinoma This is why is so important for clinicians to find a biomarker to treat these patients earlier and increase their survival. LINE-1 hyper-activation has been demonstrated in many types of cancers.

Line-1 is the most abundant human LINE. The most abundant LINE in humans is LINE-1 (L1) which constitutes at least 17% of the human genome. Indeed it is considered as a mammalian retroelement that propagates via reverse transcriptase (RT) and RNA intermediates.

The mRNA encodes two proteins, ORF1, a chaperone protein, and ORF2, which has RT and endonuclease activities.

Once L1 is activated, both ORF1 and ORF2 are expressed. Up to now, L1 activation has been assessed by analysis of DNA methylation status of the promoter region.



Methods

Healthy and cancer patients were enrolled from the University of Louisville OBGYN Physician Outpatient Center and James Graham Brown Cancer Center (controls= 24 cases= 2).

Patients should meet the following criteria:

- No previous history of cancer
- Non pregnant
- 35- 65 years old
- No comorbidities

Blood was collected and serum was separated by spinning down. ORF-1p was measured using a quantitative in-house ELISA with a polyclonal antibody in the department of pathology at University of Louisville.

Various configurations of primary antibody dilutions matched with several concentrations of secondary antibody and conjugate peptide were tested to optimize the assay for maximal delta absorbance from no protein present versus the highest calibrator concentration.

Competitive assays were carried out using streptavidin-coated 96-well microplates (Roche Diagnostics Co.) and a biotinylated conjugate of the target peptide sequence. Assay conditions were optimized using a matrix-format.

Standard curve consisting of the target sequence added as 6 increasing concentrations and three controls all prepared by spiking known concentrations of the target sequence peptide to human serum obtained from Biological Specialty Corporation (Colmar, PA).

Results

The mean ORF-1 protein concentration in the normal population (n=24) was 9.31 (SD=8.25) ng/ml. The age range The cancer patients (n=2) ORF-1 protein concentration was 0 ng/ml.

Conclusions

The results do not indicate that ORF-1 protein is increased in endometrial cancer patients. However, this study provides a foundation for future research in this field. Disadvantages of this study include a small sample population because of a lack of time to recruit healthy women and endometrial cancer patients who met the criteria for the study. This research is the beginning of a series of new studies which are going to focus in finding the relationship between different pathological conditions and the ORF-1 protein concentration

Acknowledgements

Research supported by a grant from R25-CA 134283 and the School of Medicine Summer Research Scholar Program.

A One Health Case Study: Comparison Of DNA Damage Response To Hexavalent Chromium In Alligator And Human Lung Fibroblasts

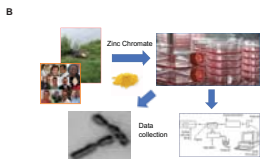
Authors: McBride, D.E., Perez, A.A., Raph S.M., Speer R.M., Croom-Perez T.J., Wise S.S., Wise Sr., J.P.

Wise Laboratory of Environmental and Genetic Toxicology, Department of Pharmacology and Toxicology, University of Louisville, Louisville, KY, United States

Research Question

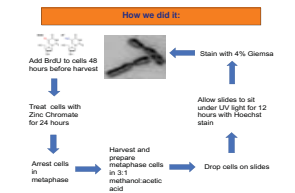
Zinc chromate is an insoluble hexavalent chromium (Cr(VI)) compound that is produced by industrial processes and has been previously shown to cause lung cancer in humans (Luppold et al.). While lung cancer is primarily associated with smoking, an estimated 10-15% of deaths annually are due to other factors, still making lung cancer in non-smokers one of the top 10 deadliest cancers in the United States and worldwide (Thun et al., 2006). Hexavalent chromium is an environmental pollutant, impacting aquatic ecosystems. To develop a better understanding of how Cr(VI) causes carcinogenesis in humans, we investigated the high-fidelity DNA repair response in human lung fibroblasts and compared this to the response in alligator lung cells. Therefore, this project investigates the question: **Do alligator lung cells exhibit more robust DNA repair during exposures to zinc chromate?**

A One Environmental Health Approach



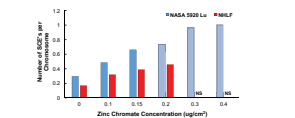
(A) We pursue a one environmental health approach, focusing on genomic instability (B) In this study, we used tissue culture and three aims to answer our research question: 1) Comparing homologous recombination in alligator and human lung fibroblasts during short term Cr(VI) exposure. 2) Comparing homologous recombination in alligator and human lung fibroblasts during long term Cr(VI) exposure; 3) Measuring the cellular uptake of Cr(VI).

Aim 1: Differences in homologous repair after 24-hour exposure



We used cell cultures of human lung fibroblasts (NHLF) and alligator lung fibroblasts (NASA 5920 Lu). Cells were treated for 24 hours at increasing Cr(VI) concentrations (0, 0.1, 0.15, 0.2, 0.3 and 0.4 $\mu\text{g}/\text{cm}^2$). The addition of BrdU allowed for harlequin staining after two replication cycles. The number of sister chromatid exchanges (SCEs) were counted at each concentration for 50 metaphases.

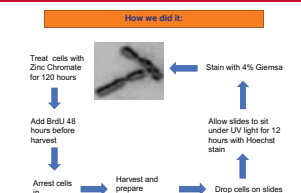
What we found:



What does it mean?

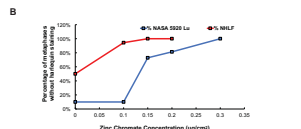
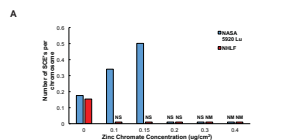
This outcome revealed that human lung fibroblasts experience greater inhibition of homologous recombination than alligator cells at higher Cr(VI) concentrations during an acute exposure, suggesting that alligator cells are better able to repair Cr(VI) induced DNA damage. If there were significantly less than 50 metaphases with harlequin staining, the value is marked as NS for "not enough SCEs". Of note, the data collection is not complete for the 0.2, 0.3 or 0.4 NASA 5920 Lu Cr(VI) concentrations and currently reflects that average number of SCEs at 21, 10 and 10 metaphases respectively. This represents one experiment out of the three replicates.

Aim 2: Differences in homologous repair after 120-hour exposure



Cells were treated for 120 hours at increasing Cr(VI) concentrations (0, 0.1, 0.15, 0.2, 0.3 and 0.4 $\mu\text{g}/\text{cm}^2$). The value is marked NS to represent insufficient SCEs. If there were no metaphases observed, the value is marked as NM for no metaphases.

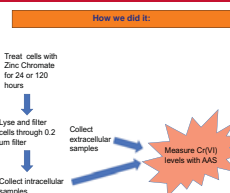
What we found:



What does it mean?

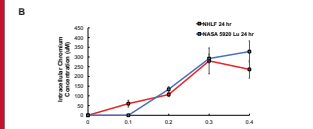
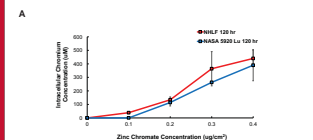
This outcome revealed that human lung fibroblasts experience greater inhibition of homologous recombination than alligator cells during prolonged zinc chromate exposure (A). Additionally, (B) depicts the percentage of observed metaphases that have harlequin staining. These data show that Cr(VI) is slowing replication in human cells to a more drastic extent than it is in alligator cells.

Aim 3: Comparing amount of intracellular uptake



We used cell cultures of human and alligator lung fibroblasts. Cells were treated with Cr(VI) for either 24 or 120 hours. Atomic absorption spectroscopy was used to measure the concentrations of zinc chromate intracellularly and extracellularly.

What we found:



What does it mean?

There was not a significant difference in intracellular concentrations of Cr(VI) at either (A) 120 hours or (B) 24 hours. This outcome revealed that differing intracellular concentrations are not causing the observed difference in homologous recombination. These data represent all three replicates for NHLF and two out three replicates for NASA 5920.

Take Home Message

This study shows that human lung fibroblasts experience greater inhibition of homologous recombination during prolonged Cr(VI) exposure and at higher concentrations than alligator lung fibroblasts. This outcome suggests alligators may have evolved better mechanisms to repair metal induced DNA damage. Additionally, these data further support the use of alligators as a species that can be used for biomonitoring Cr(VI) pollution.

Future Work

Three replicates of each experiment were performed and some are still waiting analysis at this time. Once this is complete, it will add more significance to our findings if they are found to be consistent. This study suggests that there is further investigation needed to determine how alligator cells are able to repair DNA more robustly during prolonged exposures to Cr(VI) and at high concentrations. It has been shown that the RAD51 response is suppressed in human lung cells due to subcellular mislocalization (Browning CL et al). This has not yet been studied in alligators and may offer insight into further understanding chromate induced cancers as well as options for treatment.

Further Reading

Browning CL, Wise JP Sr. Prolonged exposure to particulate chromate inhibits RAD51 nuclear import mediator proteins. *Toxicology and Applied Pharm* 2017; 101-107.

Luppold et al. Lung cancer mortality among chromate production workers. *Occup Environ Med* 2003; 451-457.

Thun MJ et al. Lung cancer death rates in lifelong nonsmokers. *Journal of the National Cancer Institute*. 2006;98(10):691-699.

Acknowledgements

Research was supported by the NCI R25 University of Louisville Cancer Education Program (R25-CA134283) and by NIEHS grant number ES018893 (J.P.W). The content is solely the responsibility of the presenters and does not necessarily represent the official views of the National Institutes of Health.

Additional funding was provided by Integrated Mission Support Services (IMSS).

Oncolytic Ability of Mutated Adenoviruses

Sean M. O'Leary, Xiao-Mei Rao M.D.¹, H. Sam Zhou, PhD.^{1,2,3}, Kelly McMasters, M.D. PhD.^{2,3}
Brown Cancer Center¹, Departments of Surgery², Pharmacology and Toxicology³
University of Louisville School of Medicine

Abstract

Introduction: Lung cancer is the leading cause of cancer deaths worldwide killing more patients than any other form of cancer. Novel lung cancer therapeutics are needed in order to combat this deadly disease. One new approach to target cancerous lung cancer cells is the use of oncolytic adenoviruses to induce the release of cancer associated antigens for subsequent uptake by dendritic cells and immune response. The adenovirus has been shown to be safe clinically, however their therapeutic efficacy is restricted by their limited viral spread and a minute natural immune response.

Objective: To determine the mutated adenovirus with the greatest cytopathic effect on each cell line as well as the effect of a Histone Deacetylase Inhibitor on virus spread in vitro.

Methods: AdWT, AdUV, Adm3, Adm60, Adm63, Adm117 and AdCycE Adenoviruses were compared in this study on A549, ED-1 and ED-6 lung cancer cell lines. Additionally, the effect of the Histone Deacetylase Inhibitor, Panobinostat, was conducted using AdUV on A549 and ED-6 cell lines. Virus titer was determined using the TCID50 method. Adenovirus spread and cell viability was quantified via crystal violet staining. Total protein concentration was determined using BSA Assay reading at a wavelength of 590 nm and protein expression of Cyclin E and Cdk was observed by western blot analysis.

Results: Adm3 and ADUV were shown to lyse A549 most efficiently, Adm117 and AdUV were shown to lyse ED-1 most efficiently, and Adm3 and Adm60 were shown to lyse ED-6 lung cancer cells most efficiently compared to the other mutated Adenoviruses. With the addition of 10-20nMol of HDACi a significant difference was observed compared to the control. However, at concentrations greater than 40nMol there was no difference observed between the control and the wells with the virus added.

Conclusions: These studies provide the groundwork that will be used in future experiments on these cell lines, as well as show the potential increase in cytopathic ability of the adenovirus with the addition of a Histone Deacetylase Inhibitor.

Introduction

- **Lung Cancer:**
 - Is the leading cause of cancer death.
 - Is in need of novel therapeutics in order to better treat the disease.
- **Oncolytic therapy:**
 - The adenovirus has been shown to be safe to use in the clinical setting
 - Therapeutic efficacy has so far been restricted by limited virus spread and minute natural immune response
- **These studies:**
 - Have shown certain mutated adenoviruses have different oncolytic potential in distinct lung cancer cell lines.
 - Point to which mutated adenoviruses should be used in future studies on the A549, ED-1 and ED-6 cell lines.
 - Reveal the potential enhancement of adenoviruses oncolytic ability with the addition of a Histone Deacetylase Inhibitor.

Results

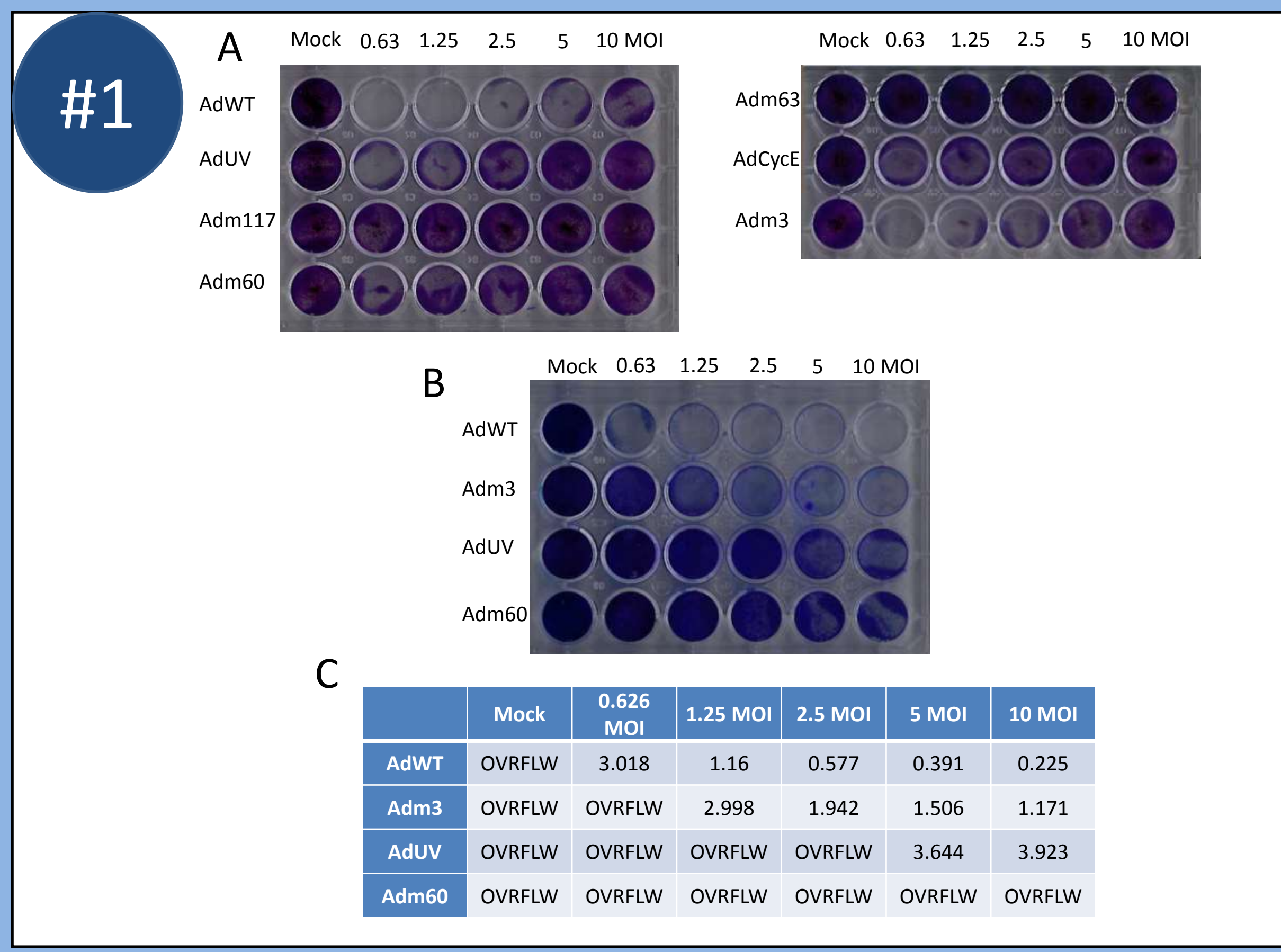


Figure 1. Adm3 and AdUV lyse the A549 lung cancer cell line more efficiently than other mutated adenoviruses. (A) A549 cells stained with crystal violet after three days' treatment with the indicated Ads and MOIs; At this stage it was determined that Adm3, AdUV and Adm60 had the greatest oncolytic potential out of the mutated adenoviruses. (B) A549 cells of the top three mutated adenoviruses stained with crystal violet after three days' treatment with the indicated Ads and MOIs; (C) BSA assay reading at a wavelength of 590 nm to analyze the crystal violet staining and determine the viruses which had the greatest oncolytic ability.

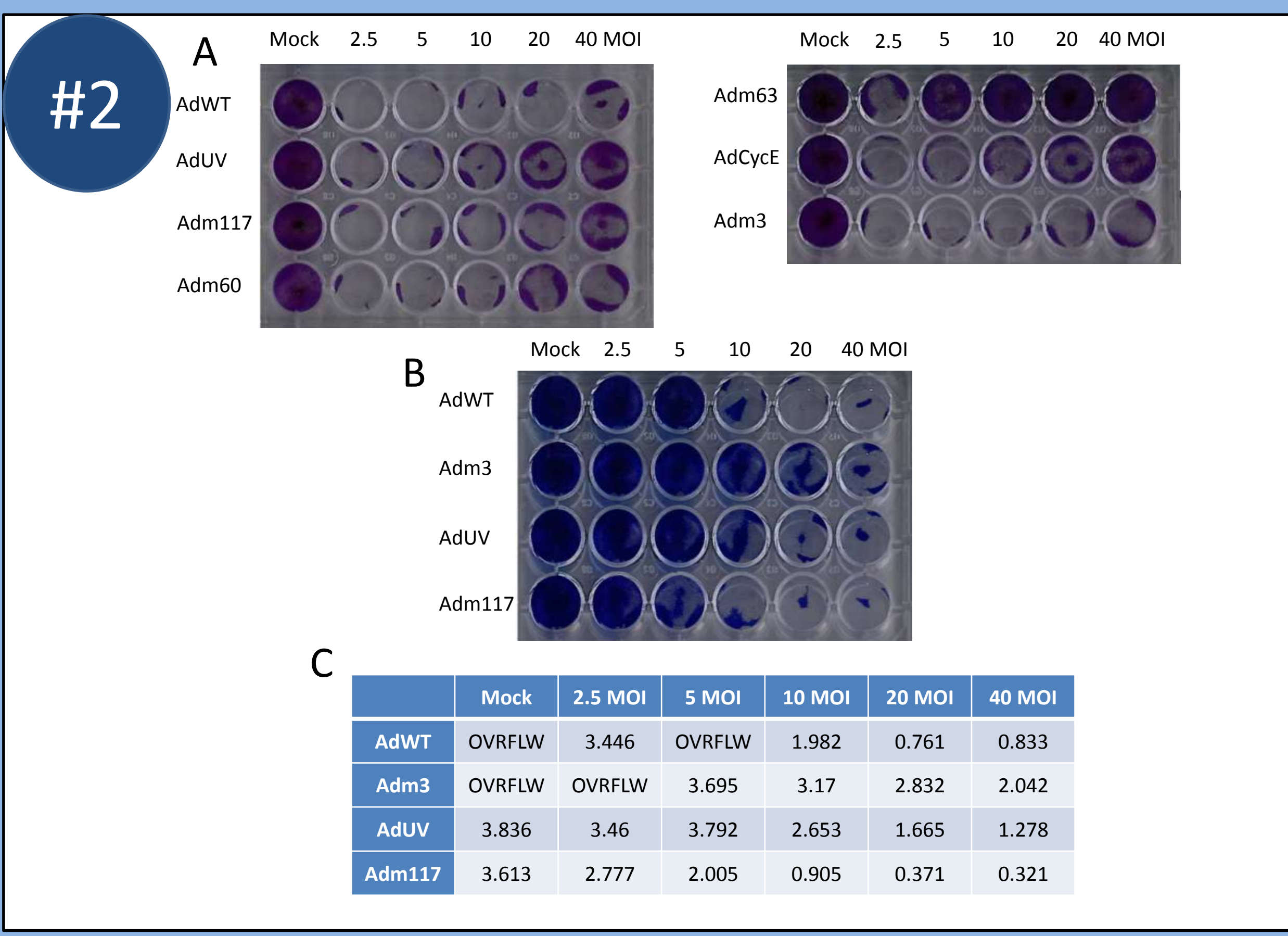


Figure 2. Adm117 and AdUV lyse the ED-1 lung cancer cell line more efficiently than other mutated adenoviruses. (A) ED-1 cells stained with crystal violet after three days' treatment with the indicated Ads and MOIs; At this stage it was determined that Adm3, AdUV and Adm117 had the greatest oncolytic potential out of the mutated adenoviruses. (B) ED-1 cells of the top three mutated adenoviruses stained with crystal violet after three days' treatment with the indicated Ads and MOIs; (C) BSA assay reading at a wavelength of 590 nm to analyze the crystal violet staining and determine the viruses which had the greatest oncolytic ability.

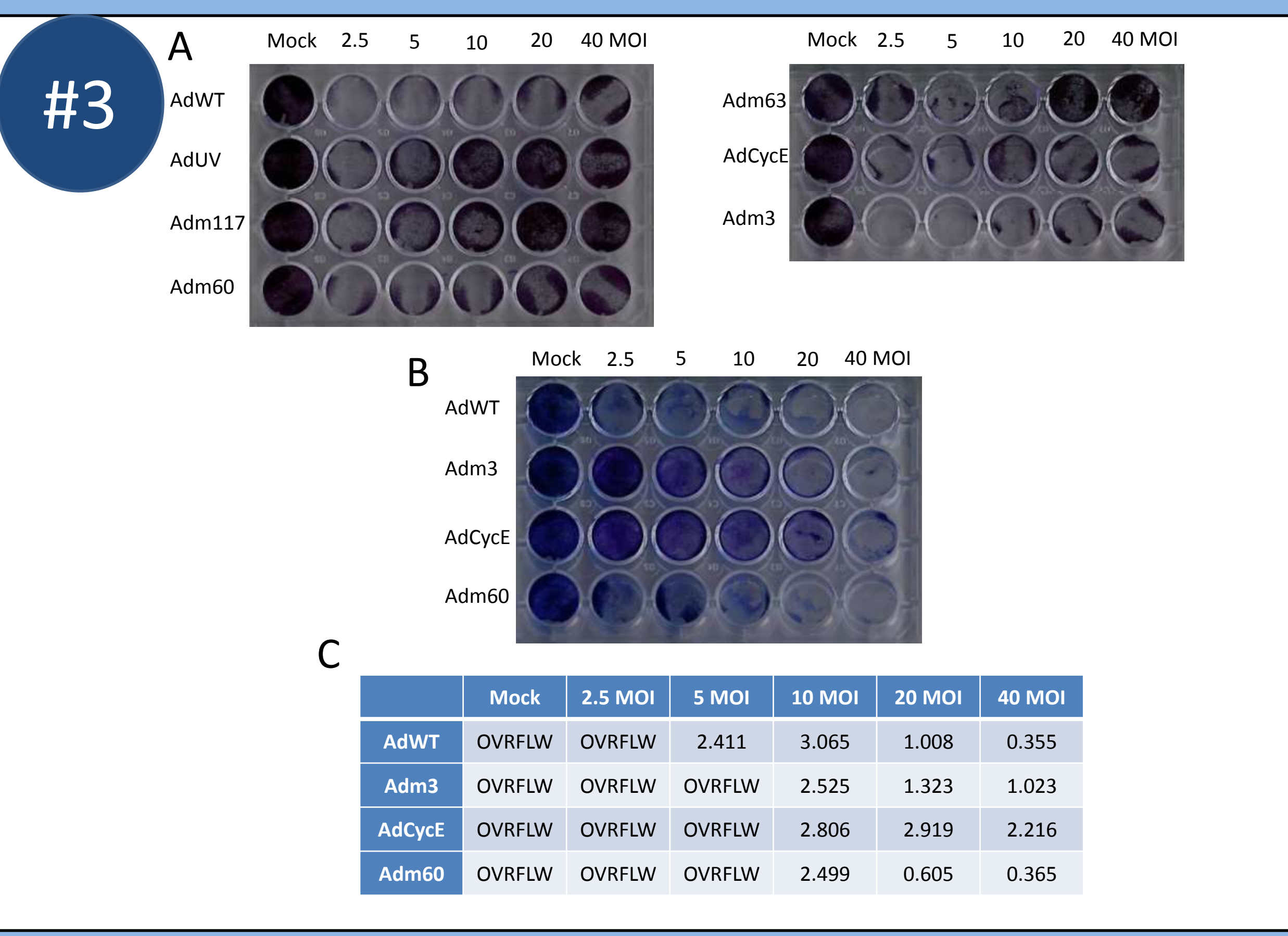


Figure 3. Adm3 and Adm60 lyse the ED-6 lung cancer cell line more efficiently than other mutated adenoviruses. (A) ED-6 cells stained with crystal violet after three days' treatment with the indicated Ads and MOIs; At this stage it was determined that Adm3, AdCycE and Adm60 had the greatest oncolytic potential out of the mutated adenoviruses. (B) ED-6 cells of the top three mutated adenoviruses stained with crystal violet after three days' treatment with the indicated Ads and MOIs; (C) BSA assay reading at a wavelength of 590 nm to analyze the crystal violet staining and determine the viruses which had the greatest oncolytic ability.

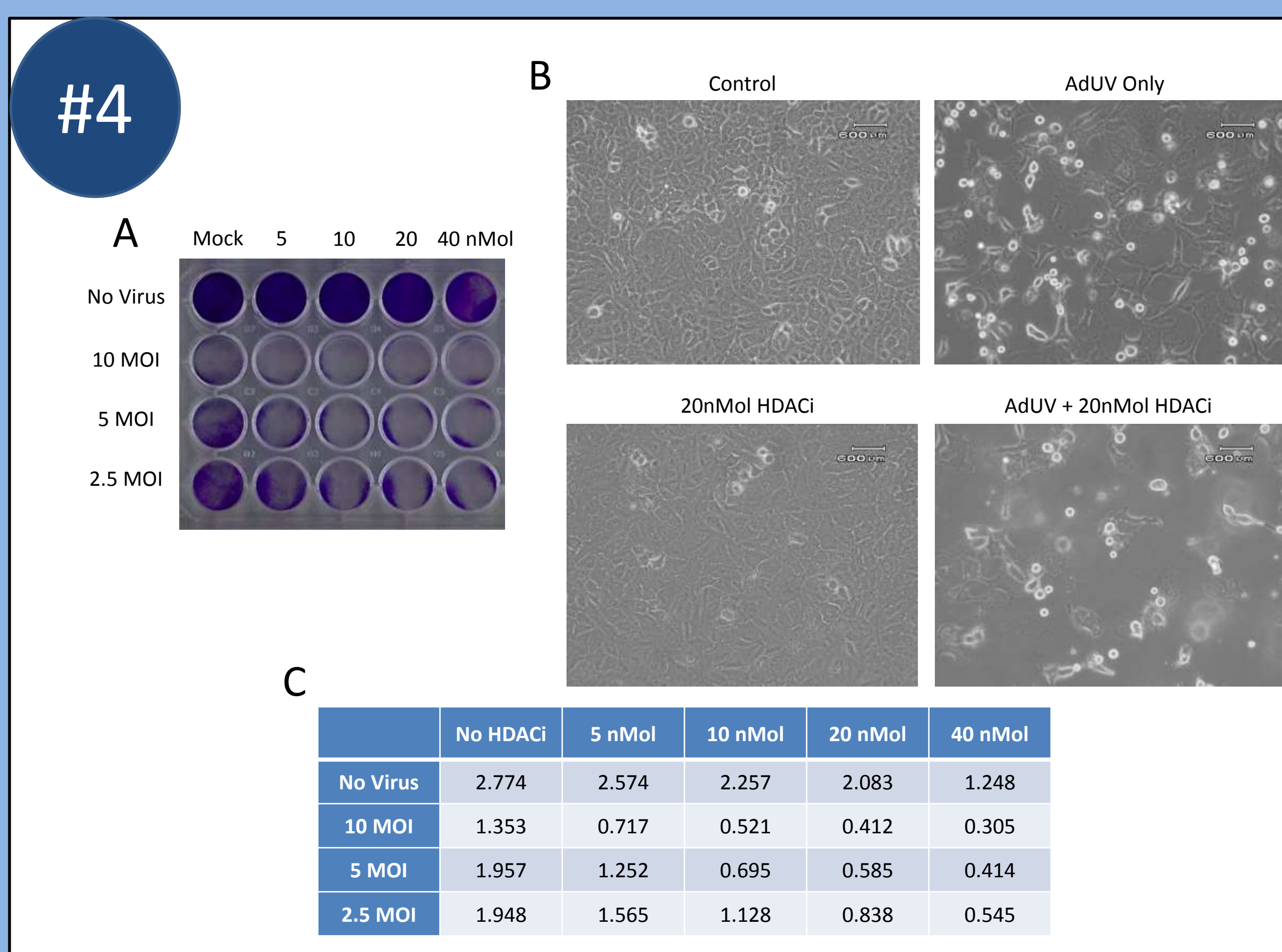


Figure 4. AdUV virus replication in A549 lung cancer cells with and without HDACi. (A) A549 cells stained with crystal violet after three days' treatment with the indicated MOIs and Histone Deacetylase Inhibitor; (B) Cytopathic and other noticeable cellular effects of the HDACi and AdUV virus on the A549 cell line were photographed at 200x total magnification after three days' treatment. (C) BSA assay reading at a wavelength of 590 nm to analyze the crystal violet staining and determine the change in cytopathic ability with the addition of an HDACi.

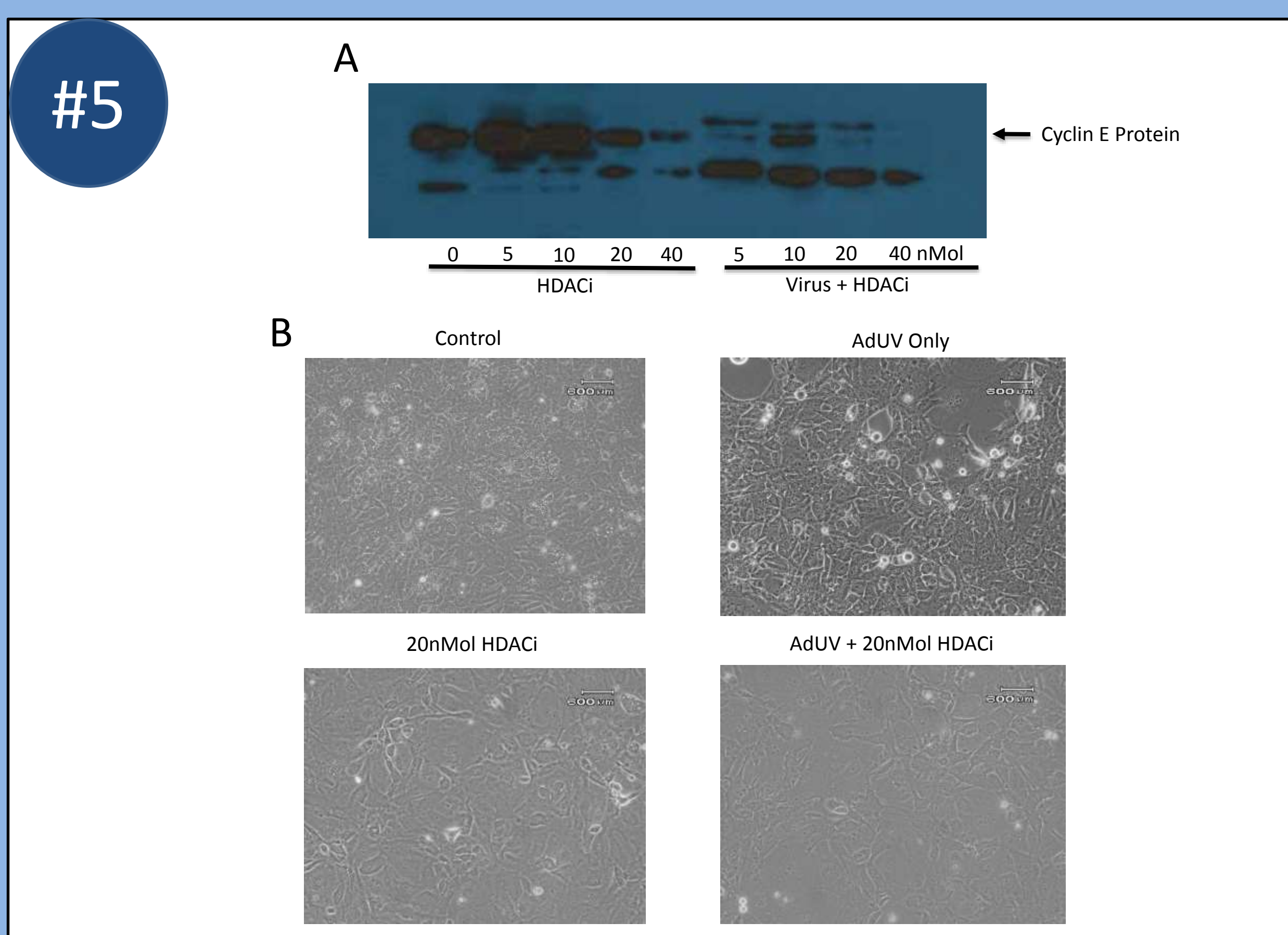


Figure 5. The effect of AdUV alone and in combination with an Histone Deacetylase Inhibitor on ED-1 lung cancer cell line protein expression and cellular features. (A) Western Blot Analysis used to determine protein expression of Cyclin E Protein and cellular growth after three days' treatment with the indicated amount of HDACi on ED-1 cells. (B) Cytopathic and other noticeable cellular effects of the HDACi and AdUV virus on the ED-1 cell line were photographed at 200x total magnification after three days' treatment.

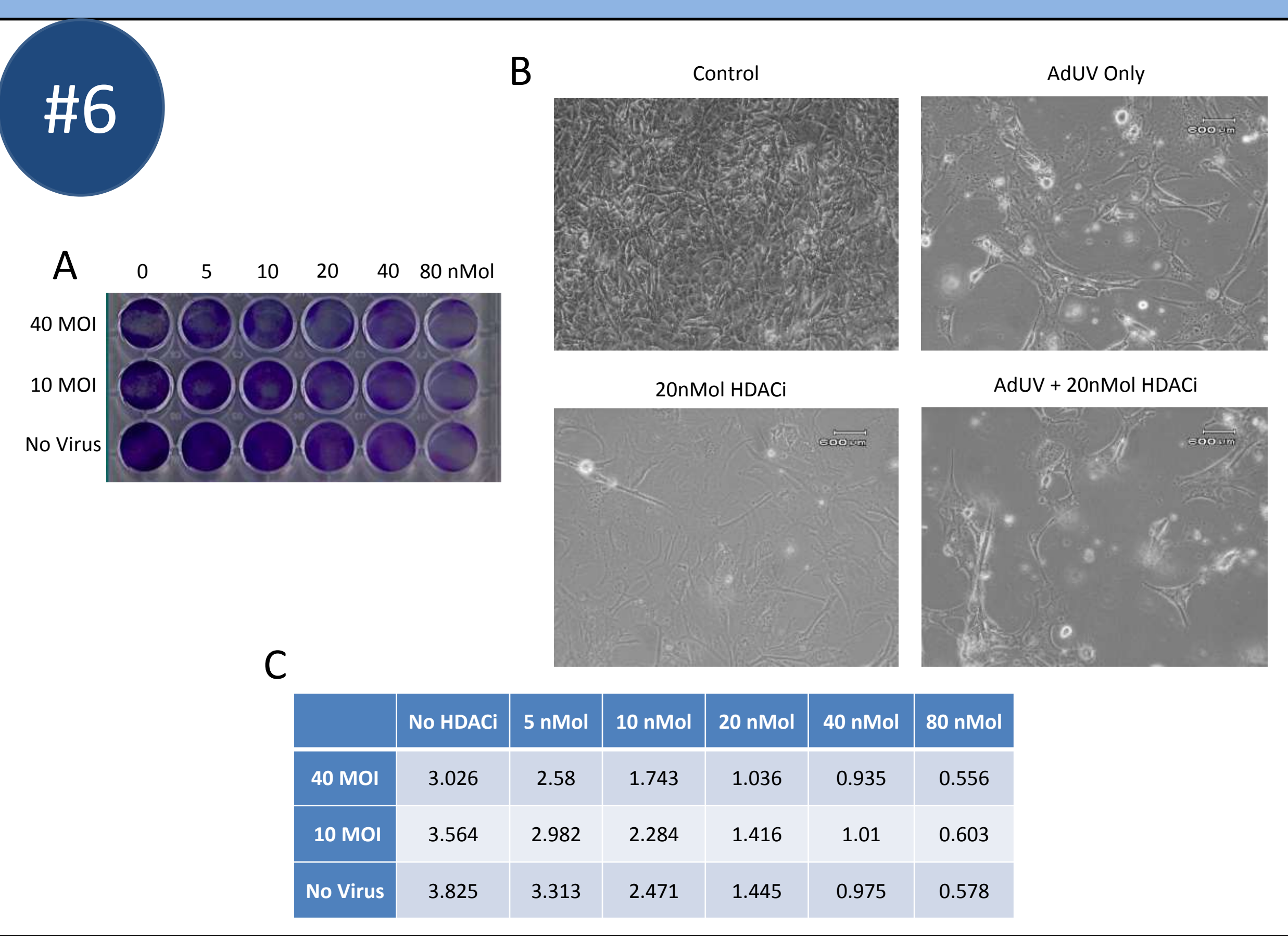


Figure 6. AdUV virus replication in ED-6 lung cancer cells with and without an Histone Deacetylase Inhibitor. (A) ED-6 cells stained with crystal violet after three days' treatment with the indicated MOIs and Histone Deacetylase Inhibitor; (B) Cytopathic and other noticeable cellular effects of the HDACi and AdUV virus on the ED-6 cell line were photographed at 200x total magnification after three days' treatment. (C) BSA assay reading at a wavelength of 590 nm to analyze the crystal violet staining and determine the change in cytopathic ability with the addition of an HDACi.

Conclusions

- Adm3 and AdUV were shown to have the highest oncolytic ability in the A549 cell line
- Adm117 and AdUV were shown to have the highest oncolytic ability in the ED-1 cell line.
- Adm3 and Adm60 were shown to have the highest oncolytic ability in the ED-6 cell line.
- The addition of 10-20nMol of a Histone Deacetylase Inhibitor revealed to enhance the oncolytic ability of the AdUV virus, while concentrations greater than 40nMol had no difference compared to the control

Acknowledgements

Research was supported by a grant from NIH R01 CA129975 (H. Sam Zhou) and the R25-CA134283 Cancer Education Program which is currently supporting me. I would also like to thank Jorge Gomez-Gutierrez and Hongying Hao for their help with these experiments and their generous instruction.

Changes in MiR-200 Family and RASSF2 Expression in Colorectal Cancer and Normal Adjacent Epithelium

Vincent T. Stephen, B.A.¹, Jane V. Carter, M.B.Ch.B., Ph.D.², Jacob C. Hallion, Maurice R. Eichenberger, M.S.², Eyas M. Hattab, M.D.³, Susan Galandiuk, M.D.^{1,2}
 University of Louisville School of Medicine¹, Price Institute of Surgical Research², Department of Pathology³

Introduction

- Colorectal Cancer (CRC) is the second leading cause of cancer-related death in the U.S.A.
- MicroRNAs (miRNA) are small non-coding RNA molecules that are involved in RNA silencing and posttranscriptional gene regulation.
- The miR-200 family (miR-200a, -200b, -200c, -141, and -429) has been widely studied in cancer, and is associated with blocking the epithelial to mesenchymal transition (EMT) in metastasis.
- One of the targets of the miR-200 family is RASSF2, which negatively regulates K-Ras, an oncogenic signaling protein.
- We have observed that the miR-200 family has been upregulated in colon cancer cell lines and that modulating miR-200 family expression in cell culture can influence K-Ras expression and cell proliferation.
- However, data from cell culture should be taken with caution, as its generalizability to physiologic conditions can be variable.
- We aimed to validate our *in vitro* findings by looking at miR-200 and RASSF2 expression in fresh frozen CRC tissue and histologically normal adjacent epithelial tissue.

Methods

- Following informed consent, tissue samples were taken from resection specimens from 5 patients with stage III CRC from the University of Louisville surgical biorepository.
- Tissue was cut and mounted on charged Histogene glass slides.
- One slide per sample was stained with hematoxylin and eosin (H&E), and cancer and normal epithelial cells were identified and marked by Pathology.
- Remaining fresh frozen tissue slides were stained and dehydrated using Arcturus® HistoGene® Frozen Section Staining Kit.
- Specific cells of interest were extracted using the ArcturusXT™ Laser Capture Microdissection System using H&E slides as reference.
- RNA was extracted and isolated from tissue using the Arcturus® PicoPure® Frozen RNA Isolation Kit for LCM.
- Quantity and Quality of purified RNA was assessed using the NanoDrop2000™ (260/280 of 1.8-2.0 was considered pure).
- Reverse Transcription followed by quantitative real-time polymerase chain reaction (qRT-PCR) was performed using specific primers and probes to the miRNAs and mRNA of interest.
- Protein was extracted from the patient resection specimens and assayed using a Western Blot.
- Data was analyzed using paired t-tests after normalizing raw data to U6 for endogenous miRNA expression, 18S for mRNA, and β-actin for protein.

Acknowledgements

Research supported by a grant from the National Cancer Institute Grant R25-CA134283, and the John W. Price and Barbara Thruston Atwood Price Trust.

Sample Makeup

Specimen Code	Tissue Type	Anatomical Site	Patient Diagnosis	Staging	Histological Grade	Gender	Age
A-T	Malignant	Colon	Adenocarcinoma	T3N1MX	II	F	66
A-N	Normal Adjacent	Colon					
B-T	Malignant	Colon	Adenocarcinoma	T3N0MX	II	M	67
B-N	Normal Adjacent	Colon					
C-T	Malignant	Colon	Adenocarcinoma	T4N2MX	II	F	57
C-N	Normal Adjacent	Colon					
D-T	Malignant	Colon	Adenocarcinoma	T3N0MX	II	F	59
D-N	Normal Adjacent	Colon					
E-T	Malignant	Colon	Adenocarcinoma	T2N1MX	II	M	55
E-N	Normal Adjacent	Colon					

Results

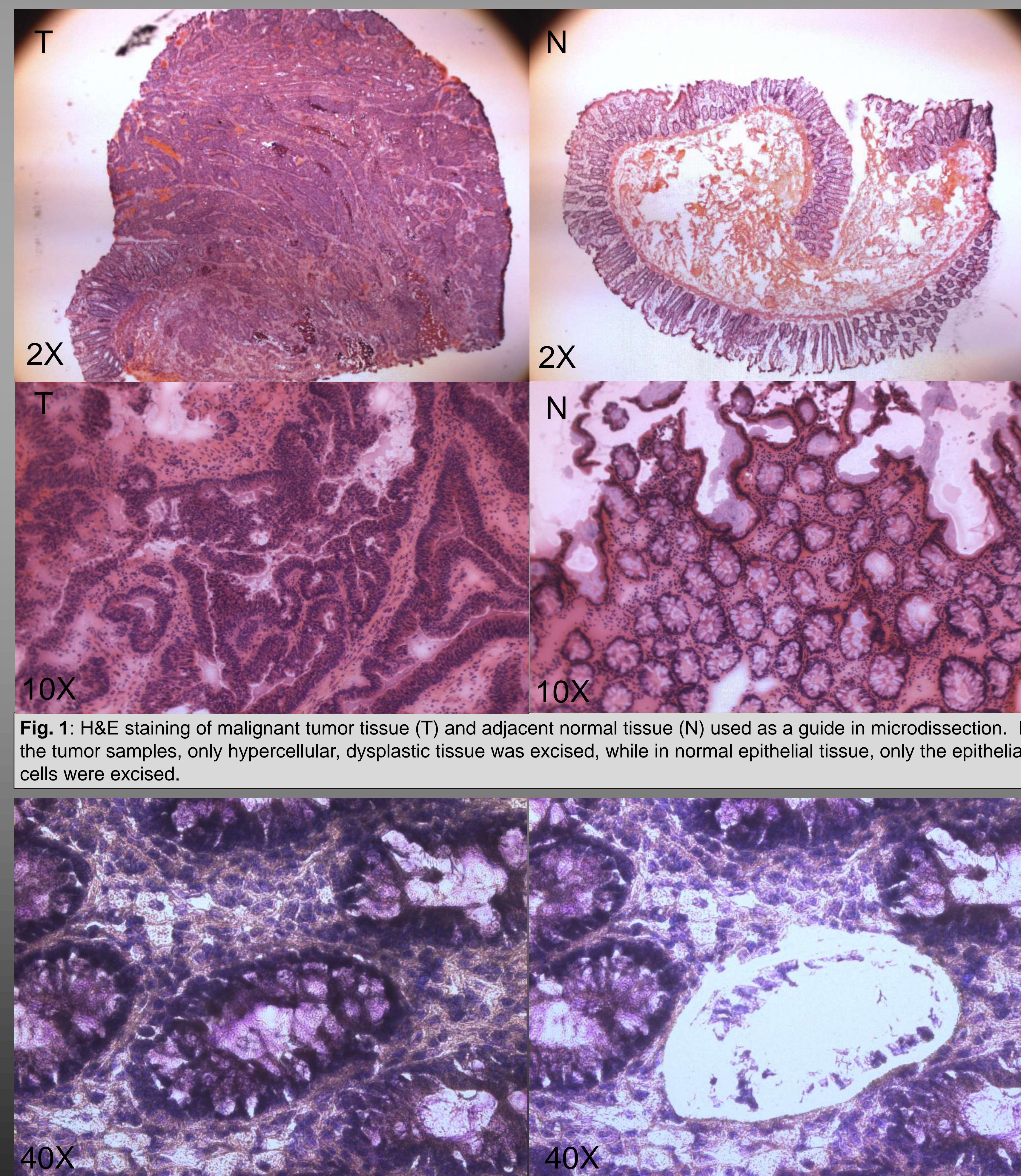


Fig. 2: Sample LCM capture of normal adjacent colon epithelium. Tissue is stained with Arcturus® HistoGene® Frozen Section Staining Kit. One glandular structure containing absorptive epithelium and goblet cells was selectively captured while stroma was left on the slide.

Results cont.

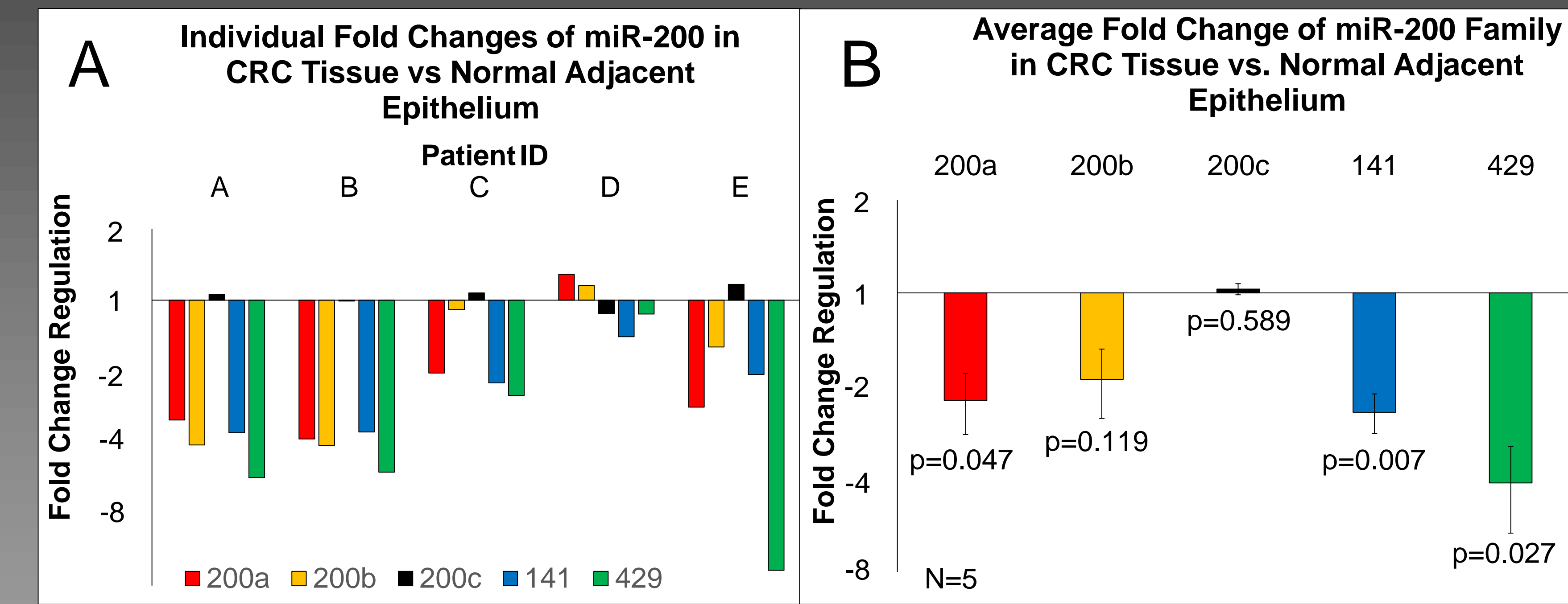


Fig. 3: (A) We observed downregulation of miR-200a and 200b in 4/5 patients, and miR-141 and 429 in all 5. We did not observe any significant change in miR-200c fold change regulation. In Fig 3B, we observed an average downregulation for miR-200a, 200b, 141, and 429, and no change in miR-200c. P-values were obtained using a paired Student's T-test after normalizing miRNA qRT-PCR raw data to U6.

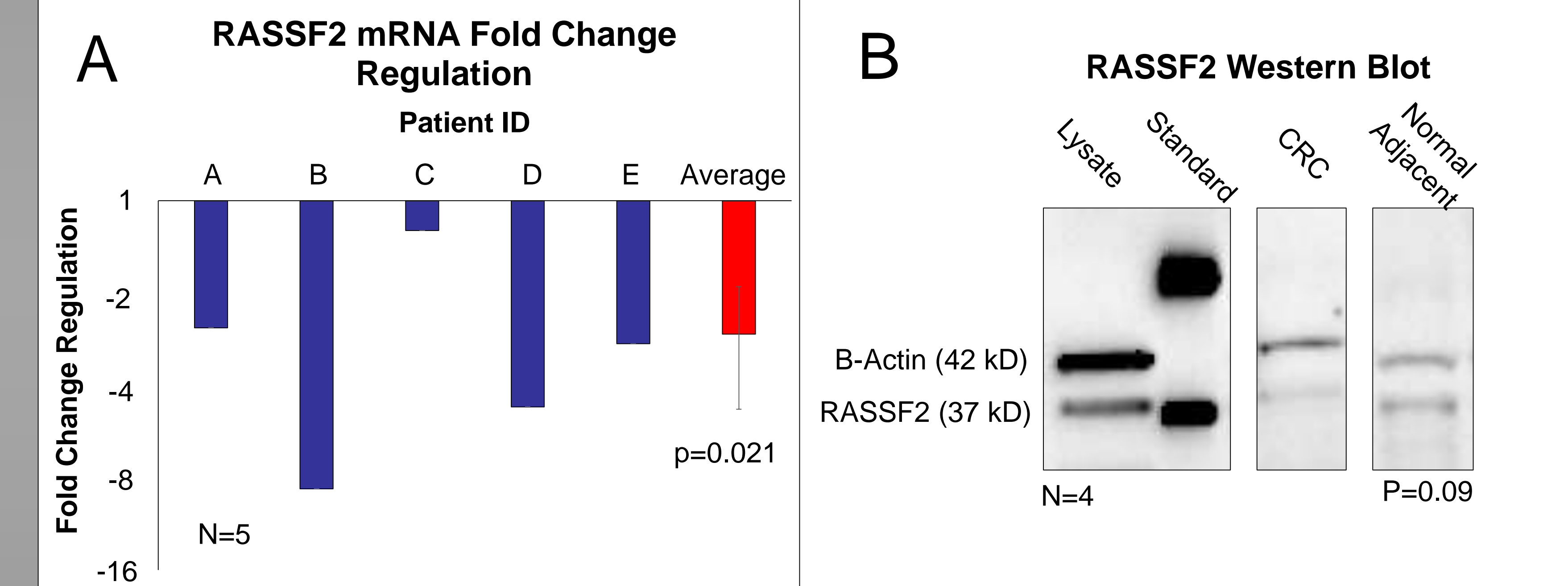


Fig. 4: (A) We observed downregulation of RASSF2 mRNA in n=5 patients, with an average fold change of -2.7 using qRT-PCR and 18S rRNA for reference. (B) A representative western blot showing RASSF2 protein downregulation using β-actin for reference. We observed a RASSF2:β-actin of 0.8 for CRC and 5.3 for normal adjacent for a -6 fold downregulation in n=4 patients. P-values were obtained using a paired Student's T-test.

Conclusions

- Although our data concerning RASSF2 are consistent with what we observed in cell culture, that for the miR-200 family are not.
- RASSF2 is a negative regulator of K-Ras, an oncogenic signaling protein. It is advantageous for cancer cells to downregulate RASSF2 expression in any environment.
- MiR-200, on the other hand, has two dichotomous roles. Upregulation may be able to block RASSF2, but downregulation helps induce EMT.
- In cell culture, there is no advantage in promoting EMT and metastasis, but this advantage exists *in vivo*, particularly in later or more aggressive cancers.
- Further investigations considering earlier stages of CRC may shed light on this discrepancy.
- Although we were able to modulate RASSF2 expression, K-RAS activation, and cell proliferation by inducing or repressing miR-200 expression in cell culture, this study identifies limitations of using miR-200 as a therapeutic target for CRC in clinical practice.

Development of novel diagnostic methodologies for diagnosis and monitoring in melanoma

Taylor Q. Nguyen¹, Alagammai Kaliappan¹, Nicholas Allen², Melissa Barousse Hall¹, Gabriela Schneider¹, Jason A. Chesney¹, Daniel Wilkey¹, Sarah K. Kendrick³, Michael L. Merchant¹, Guy N. Brock⁴, Nichola C. Garbett¹

Department of Medicine, University of Louisville¹, J.B. Speed School of Engineering, University of Louisville², School of Public Health and Information Sciences, University of Louisville³, Department of Biomedical Informatics, College of Medicine, The Ohio State University⁴

INTRODUCTION

Our lab studies multiple cancers, autoimmune and other diseases using a thermo-physical technique called differential scanning calorimetry (DSC). DSC studies changes in heat capacity over a specific temperature range of patient plasma and other biofluid samples providing a characteristic plot that we call a thermogram. Previous studies have shown that thermograms can delineate between patients with active disease and patients with no evidence of disease (NED). In this study, we applied DSC to the analysis of melanoma patient plasma samples to determine the diagnostic utility of DSC for the detection and longitudinal monitoring of melanoma. In addition, we applied mass spectrometry and ELISA analyses to determine specific biomarkers in melanoma patient samples that cause the significant changes in the bulk plasma proteome detected by DSC.

METHODS

DSC:
-Plasma thermogram data were stratified into two model groups: NED (28 patients, 86 samples) and Active disease (28 patients, 30 samples)
-Median thermograms were constructed and visualized for differences between NED and active disease
-Thermogram differences were quantified through the calculation of summary metrics: thermogram area (area), maximum peak height (height), first moment temperature (T_{FM}), heat capacity maximum of the first peak $\sim 62^{\circ}C$ (C_p^{ex} peak 1), heat capacity maximum of the second peak $\sim 70^{\circ}C$ (C_p^{ex} peak 2), peak 1: peak 2 ratio (C_p^{ex} peak 1 / C_p^{ex} peak 2) and temperature of the peak maximum (T_{max})
- Diagnostic performance of the summary metrics was determined by the construction of receiver operating characteristic (ROC) curves
- R software analytics was used to calculate metrics and ROC curves

Mass Spectrometry:

-High resolution, high mass accuracy LCMS data collected using Proxeon EASY nLC UHPLC system and Orbitrap Elite mass spectrometry in a top-10 Decision Tree approach.
-LCMS data were assigned using Proteome Discoverer v1.4.0.288 with Mascot v2.5.1 and SequestHT prior to data visualization and comparison by Scaffold Q+S v4.3.4 using an intensity based absolute quantification (iBAQ) approach.
ELISA:
- Plasma concentrations of macrophage receptor with collagenous structure (MARCO) and complement C4b were evaluated via ELISA in 32 patient samples (8 NED, 8 active disease, 9 progression)

ACKNOWLEDGEMENTS

This work was supported by funding from the National Cancer Institute (R21 CA187345 to NCG), the Kentucky Science and Technology Corporation (COMMFUND-1517-RFP-017 to NCG) and the University of Louisville Cancer Education Program / National Cancer Institute (R25 CA134283). We thank the Biorepository of the James Graham Brown Cancer Center for invaluable assistance in providing access to patient samples and clinical data for this study.

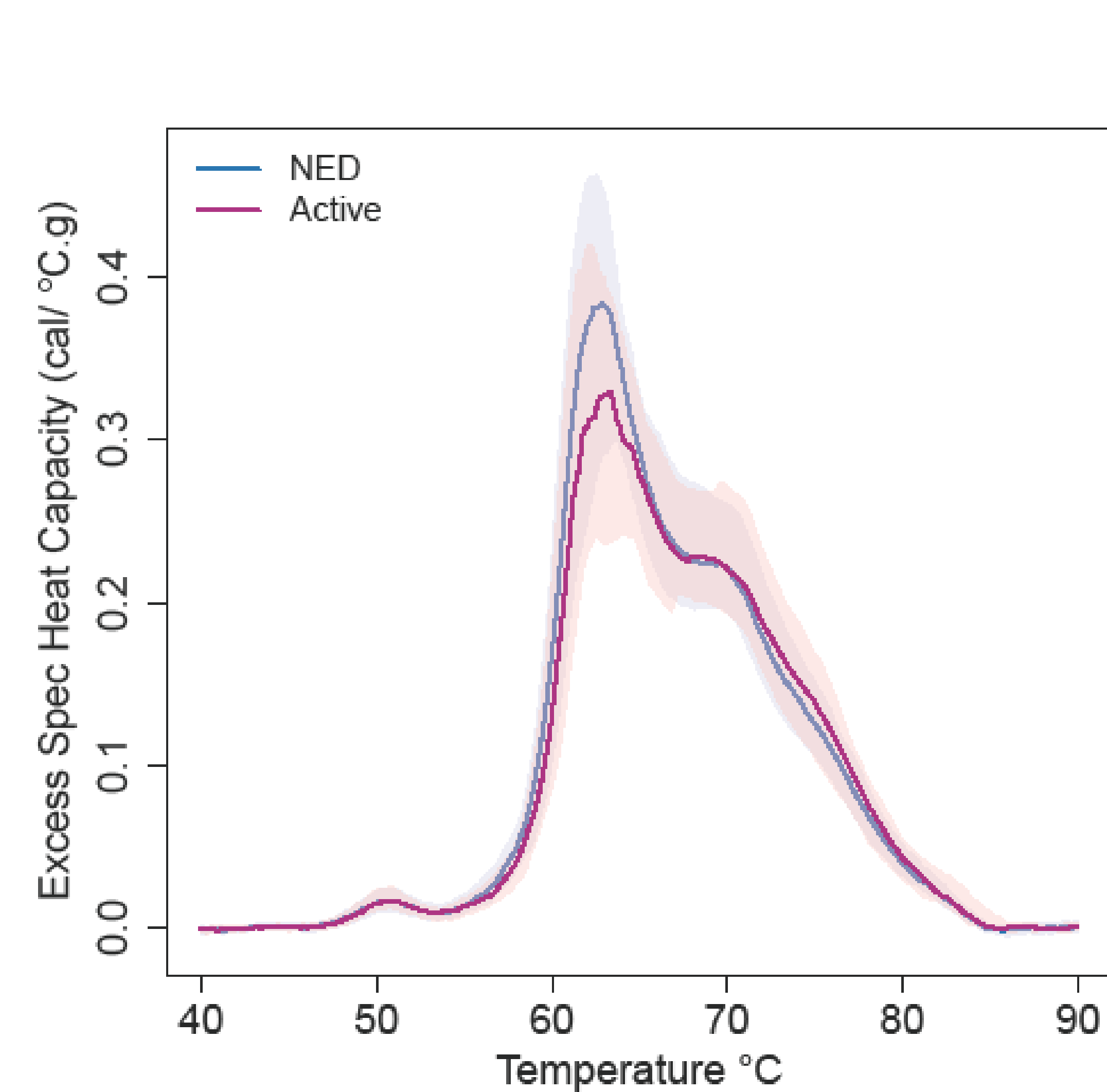


Fig. 1: Plot of median thermograms for NED and Active disease patients. Shading shows 10th and 90th percentiles.

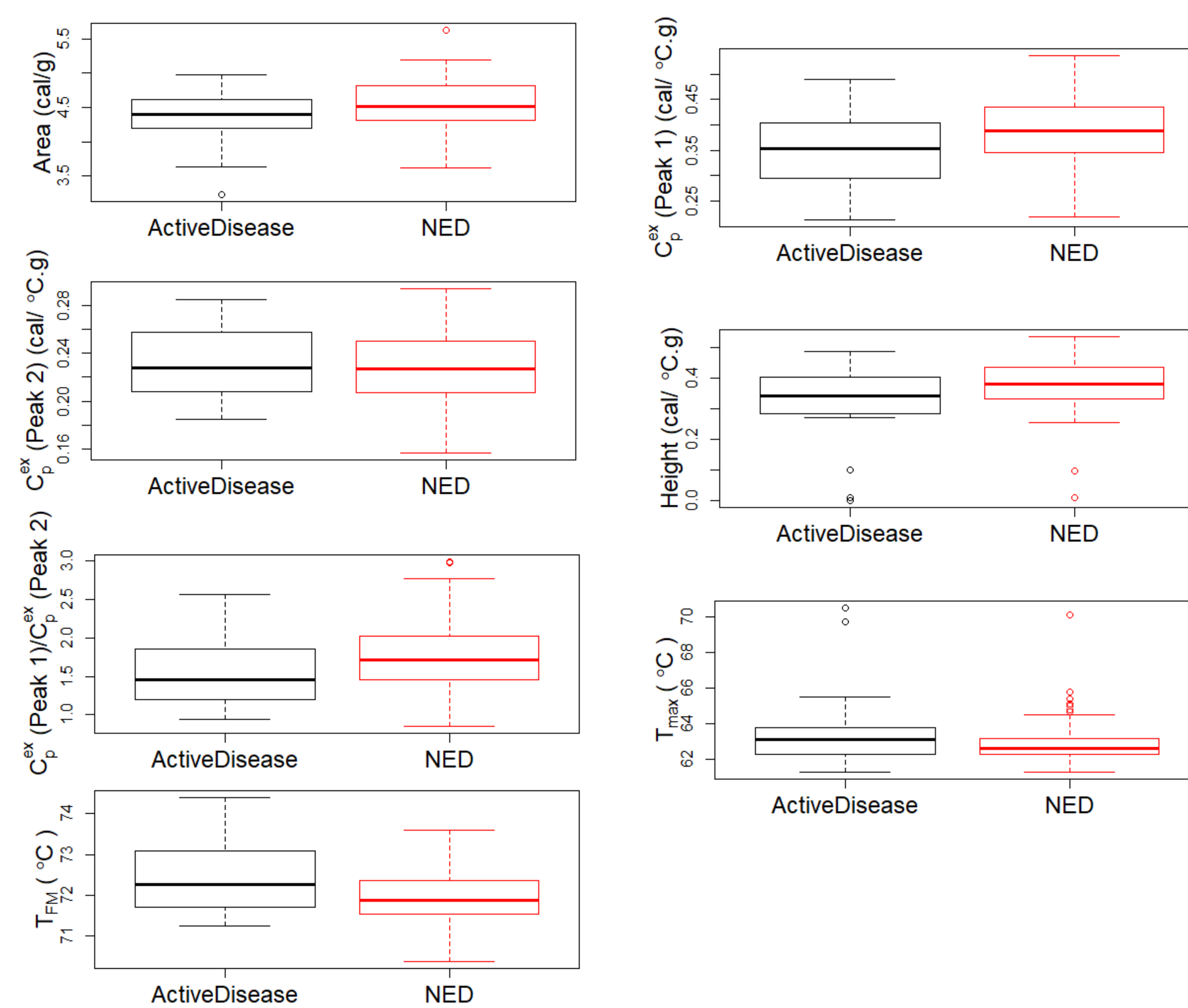


Fig. 2: Boxplots of summary metrics of NED vs Active disease patients.

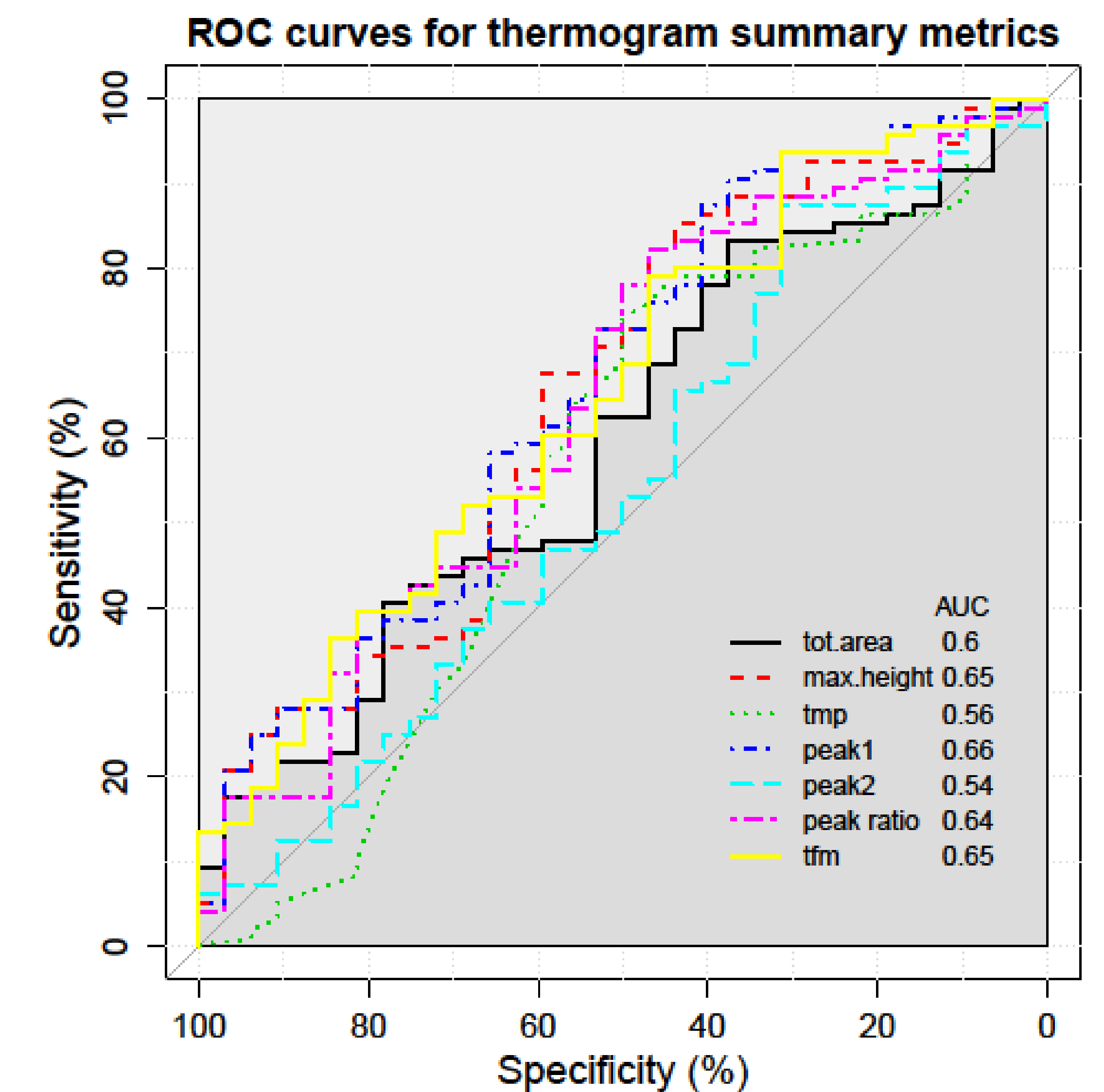


Fig. 3: ROC curves and area under the ROC curve (AUC) values for thermogram summary metrics.

#	Source?	Bio View: Identified Proteins (123) Including 1 Decoy	Accession Number	Molecular Weight	Protein Grouping Ambiguity	T-test (p-value) *p < 0.00276	Quantitative Profile	Label-free quantification of protein abundance in 10 patient plasma samples and a healthy control.									
								Ctrl	Melanoma	Ovarian	11-Ctrl	11-M1	11-M2	11-M4	11-OC1	11-OC2	11-OC3
1		Ig lambda chain V-III region LOI OS=Homo s...	sp P08748 ILV3...	12 kDa		< 0.00010	4.47E6	3.15E7	3.02E7	3.09E7	1.02	1.47	4.52	8.20	7.04	3.17	1.28
2		Isoform 2 of Alpha-2-antiplasmin OS=Homo...	sp P08697-2 A...	48 kDa		< 0.00010	6.45E5	1.14E6	1.32E6	1.83E6	9.50	3.08	1.38	2.33	5.28	4.12	3.10
3		Angiotensinogen OS=Homo sapiens GN=AG...	sp P01019 ANG...	53 kDa		0.00015	3.03E6	1.89E6	1.51E6	1.28E6	1.39	5.92	5.87	6.52	3.83	6.47	2.42
4		Ig lambda chain V-I region IIG-64 OS=Homo...	sp P01702 IYL...	11 kDa		0.00037	?	3.82E7	8.73E7	8.16E7	?	1.18	3.69	?	1.65	?	2.25
5		Haptoglobin OS=Homo sapiens GN=HP PE=L...	tr H0Y300 H0Y300...	49 kDa		0.00065	1.34E9	9.81E9	1.28E10	1.09E10	1.85	2.28	7.13	2.85	1.22	4.59	5.29
6		Macrophage receptor MARCO OS=Homo sap...	sp Q9UEW31 MARCO...	53 kDa		0.00073	?	1.67E5	1.77E5	4.09E5	?	(0)	(0)	(0)	(0)	(0)	(0)
7		Ig heavy chain V-III region VH26 OS=Homo...	sp P01764 HV3...	13 kDa		0.0011	1.89E7	5.73E7	5.25E7	6.08E7	3.47	3.27	1.43	3.51	1.79	1.05	2.12
8		Haptoglobin-related protein OS=Homo sapi...	sp P00739 HPT...	39 kDa		0.0021	5.67E8	2.99E9	4.26E9	3.48E9	5.73	9.50	2.16	1.26	3.58	2.00	2.09
9		Polymeric immunoglobulin receptor OS=Ho...	sp P01833 PIG...	83 kDa		0.011	1.04E6	2.91E6	1.12E7	1.15E7	4.35	1.44	9.68	1.27	5.78	9.78	2.47

Fig. 4: Label-free quantification of protein abundance in 10 patient plasma samples and a healthy control.

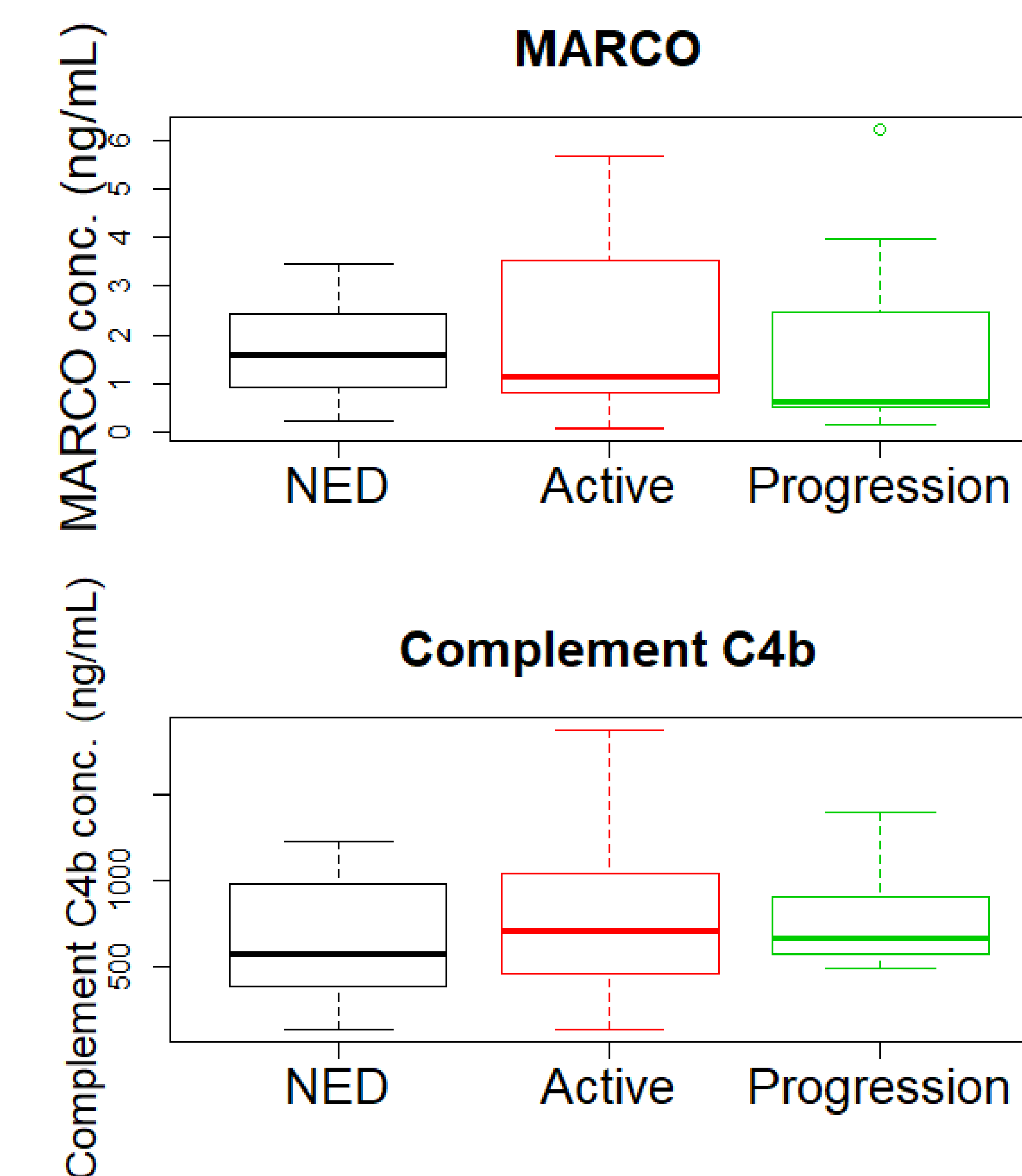


Fig. 5: Boxplots of concentrations of MARCO and C4b with respect to disease status.

FUTURE WORK

Ongoing work is addressing the use of enhanced diagnostic approaches combining multiple features of the thermogram profile. In addition, comparison of the model group metrics to longitudinal patient thermograms will allow the determination of the utility of thermograms for the monitoring of disease status. Observations of the correlation of MARCO and C4b plasma levels with tumor load results require validation in a larger sample set.

REFERENCES

- Garbett NC, Miller JJ, Jensen AB, Chaires JB. Calorimetry outside the box: a new window into the plasma proteome. *Biophys J*. 2008;94(4):1377-83.
- Garbett NC, Mekmaysy CS, Helm CW, Jensen AB, Chaires JB. Differential scanning calorimetry of blood plasma for clinical diagnosis and monitoring. *Exp Mol Pathol*. 2009;86(3):186-91.
- Garbett NC, Merchant ML, Helm CW, Jensen AB, Klein JB, Chaires JB. Detection of Cervical Cancer Biomarker Patterns in Blood Plasma and Urine by Differential Scanning Calorimetry and Mass Spectrometry. *PLoS ONE*. 2014;9(1):e84710.
- Garbett NC, Brock GN. Differential scanning calorimetry as a complementary diagnostic tool for the evaluation of biological samples. *Biochim Biophys Acta*. 2016;1860(3):381-9.
- Haouy S, Song J, Weng C, Xu J, Huang M, Huang Q, Sun R, Xiao W, Sun C. Association of decreased expression of the macrophage scavenger receptor MARCO with tumor progression and poor prognosis in human hepatocellular carcinoma. *J Gastroenterol Hepatol*. 2017;32(5):1107-1114.
- Zafar GI, Grimm EA, Wei W, Johnson MM, Ellerhorst JA. Genetic deficiency of complement isoforms C4a or C4b predicts improved survival of metastatic renal cell carcinoma. *J Urol*. 2009;181(3):1028-34.

RESULTS

- Median thermograms showed a substantially lower peak 1 and a slight right shift in peak 2 for the active disease group compared to the NED group
- Statistically significant differences ($p < 0.01$) were found for summary metrics, C_p^{ex} peak 1 and T_{FM}
- ROC curves showed moderate discrimination (AUC values of 0.7 or lower) for height, C_p^{ex} peak 1, C_p^{ex} peak 1/ C_p^{ex} peak 2 and T_{FM} . This demonstrates that single thermogram metrics have low diagnostic performance.
- A total of 362 proteins were identified across three SEC fractions of 10 patient samples. 37 proteins were identified as statistically different between melanoma and ovarian cancer samples including 33 with higher abundance in melanoma and 4 with higher abundance in ovarian cancer samples. Mean iBAQ scores were compared between melanoma and ovarian cancer samples with values interpreted with consideration to the relative abundance in the control sample. Two proteins were selected for further analysis: MARCO and complement C4b
- MARCO ELISA: concentration decreased as tumor load increased
- Complement C4b ELISA: concentration increased as tumor load increased

CONCLUSIONS

DSC shows potential for quantitatively characterizing the bulk proteome of melanoma plasma samples. Mass spectrometry analysis identified two candidate biomarkers, MARCO and complement C4b, where plasma differential abundance discriminated melanoma patient samples from ovarian cancer samples and a healthy control. Measurement of plasma concentrations of MARCO and complement C4b using ELISA analysis showed the correlation of MARCO and C4b plasma levels with tumor load.